Centennial- to millennial-scale ice-ocean interactions in the subpolar northeast Atlantic 18–41 kyr ago

I. R. Hall,[1] E. Colmenero-Hidalgo,[1,2] R. Zahn,[3,4] V. L. Peck,[5] and S. R. Hemming[6]

Received 16 November 2010; revised 14 February 2011; accepted 28 March 2011; published 30 June 2011.

[1] In order to monitor the evolution of the British-Irish Ice Sheet (BIIS) and its influence in surface ocean structure during marine isotopic stages (MIS) 2 and 3, we have analyzed the sediments recovered in core MD04-2829CQ (Rosemary Bank, north Rockall Trough, northeast Atlantic) dated between ~41 and ~18 ka B.P. Ice-rafted debris flux and composition, $^{40}Ar/^{39}Ar$ ages of individual hornblende grains, multispecies planktonic stable isotope records, planktonic foraminifera assemblage data and faunal-based sea surface temperatures (SSTs) demonstrate a close interaction between BIIS dynamics and surface ocean structure and water properties in this region. The core location lies beneath the North Atlantic Current (NAC) and is ideal for monitoring the shifts in the position of its associated oceanic fronts, as recorded by faunal changes. These data reveal a succession of BIIS-sourced iceberg calving events related to low SST, usually synchronous with dramatic changes in the composition of the planktonic foraminifera assemblage and with variations in the stable isotope records of the taxa *Neogloboquadrina pachyderma* (sinistral coiling) and *Globigerina bulloides*. The pacing of the calving events, from typically Dansgaard-Oeschger millennial timescales during late MIS 3 to multicentennial cyclicity from ~28 ka B.P., represents the build-up of the BIIS and its growing instability toward Heinrich Event (HE) 2 and the Last Glacial Maximum. Our data confirm the strong coupling between BIIS instabilities and the temperature and salinity of surface waters in the adjacent northeast Atlantic and demonstrate the BIIS's ability to modify the NAC on its flow toward the Nordic Seas. In contrast, subsurface water masses were less affected except during the Greenland stadials that contain HEs, when most intense water column reorganizations occurred simultaneously with the deposition of cream-colored carbonate sourced from the Laurentide Ice Sheet.

Citation: Hall, I. R., E. Colmenero-Hidalgo, R. Zahn, V. L. Peck, and S. R. Hemming (2011), Centennial- to millennial-scale ice-ocean interactions in the subpolar northeast Atlantic 18–41 kyr ago, *Paleoceanography*, *26*, PA2224, doi:10.1029/2010PA002084.

1. Introduction

[2] Since the discovery of millennial and faster climate variability in Greenland ice cores in the early 1990s [*Dansgaard et al.*, 1993; *Greenland Ice Core Project Members*, 1993; *Grootes et al.*, 1993], understanding of these climatic oscillations has increased rapidly. The Dansgaard-Oeschger (DO) cycles are the most prominent manifestation of climate instability in the recent geological past as they represent substantial decadal air temperature fluctuations between Greenland stadials (GSs) and interstadials (GIs) of the order of 5°–10°C in the North Atlantic region [*Dansgaard et al.*, 1993]. They coincide with variations in the properties of oceanic water masses recorded in sediment cores in the North Atlantic and beyond. These records reveal the close links between atmospheric changes and ocean dynamics [e.g., *Bond et al.*, 1992, 1993; *Cortijo et al.*, 1997; *Keigwin and Lehman*, 1994; *Vidal et al.*, 1997]. An increasing number of sediment records recovered offshore the British Isles [*Dickson et al.*, 2008; *Haapaniemi et al.*, 2010; *Hibbert et al.*, 2010; *Knutz et al.*, 2001, 2002, 2007; *Peck et al.*, 2006, 2007a, 2007b, 2008; *Peters et al.*, 2008, 2010; *Scourse et al.*, 2000, 2009] and in the Nordic Seas [*Fronval et al.*, 1995; *Kuijpers et al.*, 1998; *Lekens et al.*, 2006, 2009; *Meland et al.*, 2008; *Rasmussen et al.*, 1996a, 1996b; *Rasmussen and Thomsen*, 2004] show that the Northwestern European Ice Sheet (NWEIS) was an important element of the climate of the last glacial, in that it played a major

[1]School of Earth and Ocean Sciences, Cardiff University, Cardiff, UK.
[2]Now at Facultad de Ciencias Biológicas y Ambientales, Universidad de León, Campus de Vegazana, León, Spain.
[3]Institut de Ciencia i Tecnología Ambientals, Departament de Física, Universitat Autónoma de Barcelona, Bellaterra, Spain.
[4]Institució Catalana de Recerca i Estudis Avançats, Barcelona, Spain.
[5]British Antarctic Survey, Cambridge, UK.
[6]Lamont-Doherty Earth Observatory and Department of Earth and Environmental Sciences, Columbia University, Palisades, New York, USA.

0883-8305/11/2010PA002084

role in the freshwater release that led to disruptions in deep-water convection and influenced the Atlantic Meridional Overturning Circulation (AMOC). Of all NWEIS sectors, the British-Irish Ice Sheet (BIIS) was directly situated in, and highly dependent on, the track of moisture and heat transport derived from the North Atlantic Current (NAC) [*Hansen and Østerhus*, 2000]. As a result, the dynamics of the small-sized, fast responding BIIS were tightly coupled to variations in such transports, making nearby oceanic sediment cores highly sensitive records in which to monitor ocean-ice interactions. Evidence of BIIS growth and instability has been documented in high-resolution sedimentary sequences along its margins [e.g., *Dickson et al.*, 2008; *Knutz et al.*, 2002, 2007; *Peck et al.*, 2006, 2007a, 2007b, 2008; *Scourse et al.*, 2009] and recent modeling studies confirm that the BIIS was the dominant source of 'background' ice-rafted debris (IRD) supplied to the North Atlantic during the last glacial [*Bigg et al.*, 2010], but additional data are needed to achieve a comprehensive regional view of ocean-BIIS interactions.

[3] Here we present new high-resolution paleoceanographic records from a sediment core recovered close to the northwestern margin of the BIIS, aimed at extending results of previous records [*Knutz et al.*, 2002, 2007] well into marine isotopic stage (MIS) 3 in order to depict in fine detail the sequence of BIIS growth and decay between 41 and 18 ka B.P. We present extensive $^{40}Ar/^{39}Ar$ dating results on hornblende grains that, together with IRD composition, enable IRD to be evaluated. We also compare IRD flux with multispecies planktonic foraminifera stable isotope records and assemblage data, and with faunal-based sea surface temperature estimates (SST) as a means of closely assessing the interactions between ice sheet dynamics and surface water structure. Bringing these two approaches together enables a comprehensive and high-resolution view of the role of the BIIS in the forcing of past short-term climate variability.

2. Core Location and Oceanographic Setting

[4] Sediment core MD04-2829CQ (58°56.93′N, 9°34.30′W; 1007 cm) was retrieved at 1743 m water depth on a contourite drift located southeast of Rosemary Bank in the northern Rockall Trough during the R/V *Marion Dufresne* cruise MD141, within the SEQUOIA (Sequencing Ocean-Ice-Climate Interaction in the NE Atlantic during the Last Glacial) program [*Hall and Scourse*, 2005] (Figure 1). The core reoccupies the site of core DAPC2 that retrieved the interval 10–27 ka B.P. [*Hall et al.*, 2006; *Knutz et al.*, 2002, 2007] and was primarily targeted to extend the DAPC2 paleoceanographic records into MIS 3. Rosemary Bank is an ideal location for the recovery of continuous, high-resolution sediment records containing evidence of the variability of the BIIS, yet sufficiently far, so as not to be directly influenced by downslope processes triggered by shelf ice activity [*Sejrup et al.*, 2005], such as those shown in other cores from the nearby Barra-Donegal Fan area [e.g., *Knutz et al.*, 2001; *O'Reilly et al.*, 2007].

[5] MD04-2829CQ is also sensitively located to monitor changes of surface ocean conditions related to variability in circulation of the North Atlantic. At present, surface water circulation in the area is dominated by the northeastward flow of the warm and saline (>7°C, >35 psu) NAC, responsible for a large amount of heat and moisture transport to high latitudes, reaching as far north as the Arctic Ocean [*Hansen and Østerhus*, 2000]. The NAC meets colder and fresher (<5°C, <34.9 psu) polar waters north of the Faeroe Islands, resulting in the development of the Iceland-Faeroe Front not far from the core site, generally close to the Iceland-Scotland Ridge [*Hansen and Østerhus*, 2000; *Perkins et al.*, 1998]. Past migrations of this oceanic front due to changes in the strength of the surface currents are likely registered in our record.

[6] Two main deep water masses affect the core site: (1) a branch of the cold and saline (<3°C, <35 psu) Norwegian Sea Overflow Water (NSOW), a precursor to North Atlantic Deep Water (NADW) that enters the North Atlantic basin through the Faeroe-Shetland Channel and over the Wyville-Thomson Ridge, just northeast of the site, and (2) a boundary current of the main Northeastern Atlantic Deep Water (NEADW, recirculated upper North Atlantic Deep Water) that flows northward along the eastern European margin at 2–3 km water depth and reaches the core location regularly [*Hansen and Østerhus*, 2000; *McCartney*, 1992; *New and Smythe-Wright*, 2001; *van Aken*, 2000].

3. Materials and Methods

3.1. Core Sampling

[7] Sediment core MD04-2829CQ was sampled every centimeter across the interval 300–1008 cm, yielding a total of 708 sample slices of 1 cm thickness. Each sample was wet sieved with distilled water over a 63 μm mesh and both coarse and fine fractions recovered, dried at 40°C and weighed. Coarse (>63 μm) fractions were split into two aliquots for stable isotope, and petrological and micropaleontological analyses, which were carried out every 2 to 4 cm.

3.2. Faunal and Lithic Counts

[8] The subsamples for foraminifera faunal assemblage and lithic counts were dry-sieved over a 150 μm mesh, and the portion >150 μm was split again to yield an aliquot fraction of at least 400 planktonic foraminifera and 300 mineral grains, which were identified and counted. Planktonic foraminifera were identified following *Kennett and Srinivasan* [1983]. Relative proportions of selected taxa are presented in this work.

[9] All mineral grains >150 μm, with the exception of authigenic glauconite nodules, were considered to be IRD, and were divided into transparent quartz, haematite-coated grains, finely crystalline, cream-colored carbonate, volcanics (grey pumice, rhyolitic glass), volcanic basalt, dark grey and brown carbonates, black limestones, metamorphic and igneous rock fragments, mica flakes and hornblende grains, among the most common. The provenance of the IRD assemblage was established following the criteria outlined by *Peck et al.* [2007a]. Results are presented as fluxes in units of grains per square centimeter per kiloyear.

3.3. Sea Surface Temperature

[10] The resulting planktonic foraminifera assemblage counts were employed to estimate SST at 10 m water depth by running a transfer function based on a back propagation

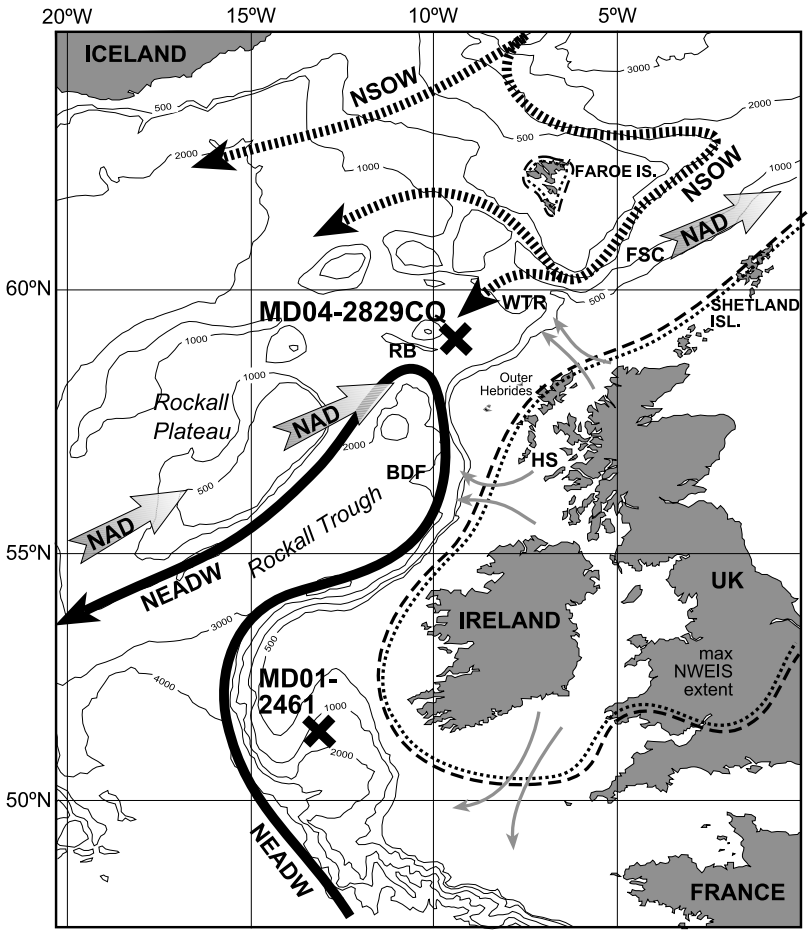

Figure 1. Bathymetric map (in meters) showing the location of cores MD04-2829CQ and MD01-2461 and the approximate path of present-day surface and deep-water masses. NAD, North Atlantic Drift (grey arrows); NSOW, Nordic Seas Overflow Water (dashed black arrows); NEADW, Northeastern Atlantic Deep Water (black arrows); FSC, Faroe-Shetland Channel; WTR, Wyville-Thomson Ridge; RB, Rosemary Bank; BDF, Barra and Donegal Fans; and HS, Hebrides Shelf. Double dashed black lines indicate the estimated maximum extent of the northeastern European and Faroe Islands ice sheets during the Last Glacial Maximum, and grey arrows indicate approximate location of the associated ice streams (references in text).

artificial neural network (ANN) [*Malmgren et al.*, 2001] trained on the North Atlantic MARGO Project data set [*Kucera et al.*, 2005]. The same data set was used to apply a Modern Analogue Technique (MAT) [*Prell*, 1985] to the faunal counts. For the ANN, a set of ten neural networks was considered, providing 10 different mean annual SST reconstructions, which were averaged to estimate the SSTs and standard deviations from the calibration data set. The MAT was applied using a set of ten modern analogs, allowing the calculation of a similarity index for MAT SSTs.

3.4. Dating of $^{40}Ar/^{39}Ar$ on Hornblende Grains

[11] A total of 421 individual hornblende fragments from the >150 μm fraction were picked when present and analyzed to provide for provenance data of IRD. Grains from the same horizon were grouped in the same sample, yielding a total of 184 samples covering the interval from ~18 to ~40 ka B.P., that were sent to the Cd-lined core facility (CLICIT) at the Oregon State University reactor (USA) for their coirradiation with the hornblende monitor standard Mmhb (525 Ma [*Samson and Alexander*, 1987]). Argon activity analyses were performed at the Ar Geochronology Laboratory, Lamont-Doherty Earth Observatory (LDEO, USA), where individual grains were fused with a CO_2 laser and ages were calculated from the resulting Ar isotope ratios, corrected for mass discrimination, interfering nuclear reactions, procedural blanks and atmospheric Ar contamination following the standard procedure of *McDougall and Harrison* [1999].

3.5. Isotope Measurements

[12] Aliquots for stable isotope analyses were dry-sieved over 250 and 355 μm meshes. Around 10–15 specimens of the planktonic foraminifera *Neogloboquadrina pachyderma* (sinistral coiling), mostly the encrusted type, were obtained every 2 cm, while up to 15–20 individuals of *Globigerina bulloides* were picked when possible. Around 25 specimens of *Turborotalita quinqueloba* (>150 to <250 μm) were also

Table 1. AMS Radiocarbon Ages for MD04-2829CQ and Their Calibrated Correspondence as Well as Their Calendar Age According to the Tuned-to-GISP 2 Age Model and the Difference in Years Between Both Age Models as Plotted in Figure 3b

Laboratory Code	Depth (cm)	Material	^{14}C Age (years)	Error Age (±1σ years)	Calendar Age (cal years B.P.)[a]	Error Age (± years)	Age GISP 2 (cal years B.P.)	Difference Age Models (years)
SUERC-8793	312.5	*N. pachyderma* l.c.	16,732	65	19,450	86	18,498	952
SUERC-8794	376.5	*N. pachyderma* l.c.	17,254	69	20,024	107	19,380	644
SUERC-8795	391.5	*N. pachyderma* l.c.	17,382	70	20,174	91	19,595	579
SUERC-8797	422.5	*N. pachyderma* l.c.	17,706	73	20,470	94	20,024	446
SUERC-8798	438.5	*N. pachyderma* l.c.	17,992	76	20,806	128	20,242	564
SUERC-8799	457.5	*N. pachyderma* l.c.	18,231	78	21,127	141	20,373	754
SUERC-8802	495.5	*N. pachyderma* l.c.	18,312	80	21,239	146	20,649	590
SUERC-8803	510.5	*N. pachyderma* l.c.	18,569	83	21,626	165	20,758	868
SUERC-8804	534.5	*N. pachyderma* l.c.	18,670	82	21,802	162	21,159	643
SUERC-8805	544.5	*N. pachyderma* l.c.	18,804	84	22,012	132	21,436	576
SUERC-8807	560.5	*N. pachyderma* l.c.	19,597	92	22,793	130	21,879	914
SUERC-8808	592.5	*N. pachyderma* l.c.	20,328	101	23,813	143	22,764	1049
SUERC-8809	618.5	*N. pachyderma* l.c.	20,512	104	24,021	132	23,252	769
SUERC-8812	636.5	*N. pachyderma* l.c.	20,696	106	24,203	121	23,539	664
SUERC-8813	648.5	*N. pachyderma* l.c.	21,383	117	25,107	178	23,911	1196
SUERC-8814	664.5	*N. pachyderma* l.c.	21,447	116	25,190	171	24,408	782
SUERC-8815	720.5	*N. pachyderma* l.c.	23,505	151	27,726	220	26,441	1285
SUERC-8816	762.5	*N. pachyderma* l.c.	24,779	174	29,160	234	28,112	1048
SUERC-8817	784.5	*G. bulloides*	25,711	197	30,465	269	28,792	1673
SUERC-10904	807.5	*N. pachyderma* l.c.	26,480	146	31,318	210	30,017	1301
SUERC-10899	816.5	*N. pachyderma* l.c.	26,963	154	31,839	224	30,679	1160
SUERC-10900	880.5	*N. pachyderma* l.c.	30,073	223	35,092	254	34,146	946
SUERC-10901	916.5	*N. pachyderma* l.c.	32,909	306	37,905	344	36,755	1150
SUERC-10902	950.5	*N. pachyderma* l.c.	35,136	399	40,092	421	39,020	1072

[a]Converted using the online calibration program of *Fairbanks et al.* [2005], January 2007 version, and assuming a constant 400 year marine reservoir correction.

picked every 2 cm in the interval 780–830 cm. Prior to analyses samples were submerged in hydrogen peroxide (3%) for 30 min and briefly ultrasonicated in ethanol. Excess liquid and residues were quickly removed and the tests dried at low temperatures (40°C). *T. quinqueloba* samples were not cleaned or crushed prior to analysis due to their fragility and small size. All samples were analyzed on a ThermoFinnigan MAT 252 mass spectrometer coupled to a fully automated CARBO Kiel carbonate preparation device at the Stable Isotope Laboratory of Cardiff University (UK). Isotope results are reported in standard delta notation relative to Vienna Pee Dee Belemnite (VPDB), using NBS-19 for calibration. The external reproducibility of the δ^{18}O determination is ±0.06 ‰.

[13] Possible contamination of isotopic results by clay-size dolomitic carbonate fragments attached to shell walls [*Hodell and Curtis*, 2008] was reduced to a minimum since all *N. pachyderma* sin. samples from cream-colored carbonate bearing IRD horizons (mainly HE 2 and HE 4) were crushed before cleaning, as well as *G. bulloides* samples corresponding to HE 4.

[14] Extra analyses on specimens from intermediate horizons within intervals with anomalous isotopic values (e.g., spikes in the *G. bulloides* δ^{18}O record) were performed when possible, yielding a final 1 cm resolution on those specific intervals. All paleodata will be publicly available through the World Data Centre for Marine Environmental Sciences (http://www.wdc-mare.org; http://www.pangaea.de).

4. Age Model

[15] The chronostratigraphic framework of core MD04-2829CQ is based on the calibration to calendar years (cal years B.P.) of 24 AMS ^{14}C dates determined from monospecific samples containing more >1000 specimens (equivalent >10 mg of carbonate) of *N. pachyderma* sin. or *G. bulloides* (Table 1). Samples for dating were selected from sections where abundance of either taxon maximized in order to minimize the influence of bioturbation [*Bard et al.*, 1987]. AMS ^{14}C analyses were run at the NERC Radiocarbon Laboratory facility (East Kilbride, UK). Carbon-14 dates were converted to calendar years using the online calibration program of *Fairbanks et al.* [2005] (www.radiocarbon.ldeo.columbia.edu) with its January 2007 database, applying a 400 year correction for global marine reservoir age [*Stuiver et al.*, 1998] that coincides with modern local estimates for the area between 40°–70°N in the North Atlantic [*Bard*, 1988; *Butzin et al.*, 2005] (Figure 2). The resulting age model was then fine tuned and extended beyond current AMS ^{14}C coverage by correlating relative abundance of *N. pachyderma* sin. to the GISP 2 Greenland ice core $\delta^{18}O_{ice}$ record [*Grootes and Stuiver*, 1997] (Figures 2 and 3a and Table 2.). The GISP 2 record has estimated age uncertainties of about ±2% for the age interval studied here [*Meese et al.*, 1997], and shows a good long-term agreement with the more recent NGRIP ice core [*Svensson et al.*, 2008]. Therefore it was selected for correlation instead of the NGRIP in order to facilitate comparison of our results to those from cores MD01-2461 and DAPC2, also tuned to GISP 2 [*Knutz et al.*, 2007; *Peck et al.*, 2006, 2007a, 2007b, 2008]. The name convention of the INTIMATE group for the GSs and GIs is used [*Lowe et al.*, 2007].

[16] Tuning *N. pachyderma* sin. abundance maxima to Greenland stadials is a common procedure in North Atlantic records [e.g., *Bond et al.*, 1993; *Bond and Lotti*, 1995; *Knutz et al.*, 2007; *Peck et al.*, 2006] and is based on the obser-

Table 2. Depths and Corresponding Calendar Ages of the Tie Points Used for the Fine Tuning of the Radiocarbon-Based Age Model to the GISP 2 Oxygen Isotope Record[a]

MD04-2829CQ Depth of Pointers (cm)	Age GISP 2 (cal years B.P.)	Stratigraphic Position	Sedimentation Rates (cm kyr^{-1})
300	18,334	GS 1, top of record	–
369	19,280	GS 1	72.90
434	20,215	GS 1	69.87
522	20,851	GS 1	137.62
600	23,017	base GI 2	36.13
633	23,475	base GI 2	71.69
687	25,151	GS 3	32.20
759	28,053	base GI 3	24.87
794	29,132	base GI 4	32.34
815	30,681	base "DO 4.1"	13.59
826	32,312	base GI 5	6.75
864	33,672	GI 6	27.88
879	34,146	base GI 6′	31.73
897	35,281	base GI 7	15.82
936	38,467	base GI 8	12.25
960	39,492	HE4	23.53
1007	41,153	top GI 10, base of record	28.24

[a]Explanation and references in text and in Figure 3. The approximate stratigraphic position of the selected intervals (Figure 3a) and the partial sedimentation rates (Figure 2) are also included.

vation that this taxon is dominant in present-day polar and subpolar assemblages [*Bé*, 1977; *Ruddiman and McIntyre*, 1981]. Hence it is considered a proxy for both arctic water masses with seasonal ice cover [*Johannessen et al.*, 1994] and polar water masses with perennial sea ice cover [*Elliot et al.*, 1998; *Kuijpers et al.*, 1998; *Pflaumann et al.*, 1996].

[17] The resulting chronostratigraphic framework (Figure 2) shows that our records span an interval of about 23 kyr, extending between mid MIS 3 (~41.1 ka B.P.) and mid MIS 2 (~18.3 ka B.P.). The age model has independently been constrained by the identification of the Laschamp excursion (~41 ka B.P.) [*Lund et al.*, 2005] in the magnetic record (E. Moreno, personal communication, 2010). Mean sedimentation rates for the studied interval are approximately 31 cm kyr^{-1}, yielding a mean time step of ~65 years for each 2 cm interval, with maximum rates of up to 137 cm kyr^{-1} recorded during MIS 2. Sedimentation rates increase from ~26 ka B.P. toward the Last Glacial Maximum (LGM), in a similar fashion to those recorded in nearby cores MD95-2006, DAPC2 and ENAM32 [*Knutz et al.*, 2001, 2007; *Lassen et al.*, 1999] and sites in the southern Norwegian Sea [*Nielsen et al.*, 2007; *Rasmussen et al.*, 1996b], probably reflecting a combination of changing bottom current intensity and terrigenous sediment supply to the core site.

[18] Significant temporal discrepancies between the initial ^{14}C-calibrated and the calendar year timescale derived from tuning to the GISP 2 age model (Figure 2) suggest that local marine reservoir ages (ΔR) have shifted within a range of ~430 to ~1700 years, far larger than the modern global average 400 year reservoir correction (Figure 3b). Mean implied ΔR values during MIS 2 are typically ~700 years, while in MIS 3 the divergence increases to ~1000 years. Maximum ΔR values are found close to H events. High reservoir ages during colder periods are systematically registered in records recovered off the British Isles [*Knutz et al.*, 2007; *Lekens et al.*, 2006; *Peck et al.*, 2006] and in other regions of the glacial North Atlantic, due to a combination of sea-ice and meltwater induced reduction of air-sea gas exchange, ventilation and isotope equilibration [*Austin et al.*, 1995; *Bard et al.*, 1994; *Voelker et al.*, 1998; *Sarnthein et al.*, 2007; *Waelbroeck et al.*, 2001]. Increased contribution of ^{14}C-depleted Antarctic waters reaching the high latitude North Atlantic [*Cao et al.*, 2007] possibly have added to the elevated reservoir ages. The effect of these differences apparently decreases toward lower latitudes, deglacial warm periods and the Holocene [*Cao et al.*, 2007; *Waelbroeck et al.*, 2001].

5. Results

5.1. Abundance Distribution of Planktonic Foraminifera

[19] Changes in the relative abundances of planktonic foraminifera closely reproduce the variability seen in the GISP 2 $\delta^{18}O_{ice}$ record (Figure 4). Large fluctuations in the assemblage composition characterize the period between 41 and 27 ka B.P., in accordance with the high-amplitude GS-GI cycles 4 to 11. *N. pachyderma* sin. dominates during HE and GSs, while transient increases of temperate/subtropical taxa (e.g., *Globorotalia scitula*) mark the warmer GIs, dominated by *G. bulloides* and *T. quinqueloba*. Abundance of *N. pachyderma* (dextral coiling; abundances not shown here) also increases during GIs but never reaches values above 5%.

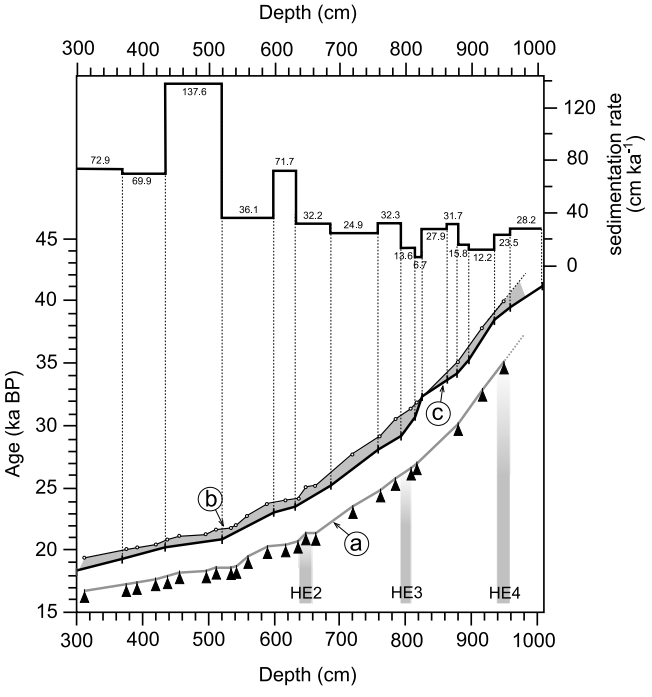

Figure 2. Age models of core MD04-2829CQ. (a) Solid triangles, raw radiocarbon AMS dates; (b) thin black line, AMS ^{14}C dates calibration to calendar ages; and (c) thick black line, tuned-to-GISP2 age model. The grey area evidences the divergence between the AMS ^{14}C calibrated and the tuned-to-GISP2 age models. The sedimentation rates according to the tuned-to-GISP2 age model are also plotted. Positions of HE 2–4 are included for reference.

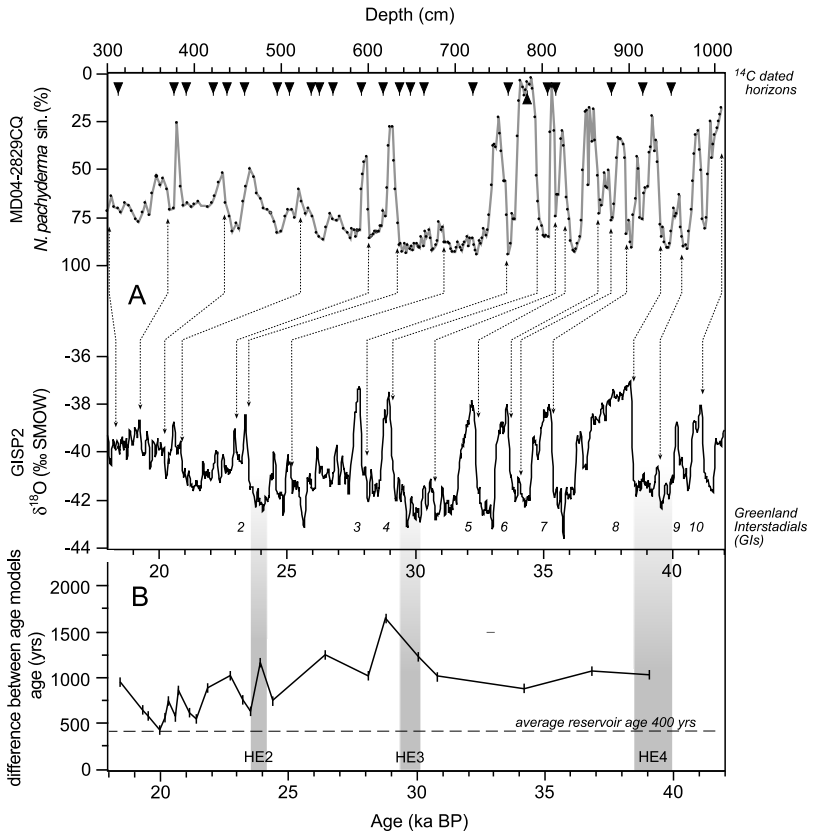

Figure 3. (a) Correlation of the relative abundance of *N. pachyderma* sin. recorded in core MD04-2829CQ with the GISP 2 oxygen isotope record [*Grootes and Stuiver*, 1997]. Dotted arrows connect tie points used for the correlation, while black triangles indicate the horizons dated with AMS ^{14}C. (b) Difference in years between the calibrated AMS ^{14}C ages and the calendar ages for the same horizons as given by the tuned-to-GISP2 age model. The horizontal dashed line marks the average modern mean reservoir age. The position of HE 2 to HE 4 is plotted for reference.

[20] *N. pachyderma* sin. is the dominant taxon between 27 and 18 ka B.P., showing small abundance shifts during the LGM interval coincident with centennial-scale climate variations observed in Greenland. Major exceptions are two brief abrupt increases of the cold/temperate species *Turborotalita quinqueloba* and *G. bulloides* coincident with GI 2.

5.2. Faunal-Based Sea Surface Temperatures

[21] SST from ANN and MAT techniques generated very similar records and values, with the occasional exception, for example peak warmth during GI 3 and 4, where ANN estimates suggest higher temperatures up to 3°C higher than MAT (Figure 4). A few levels from both reconstructions, however, are affected by no-analog situations, as indicated by MAT similarity values below 0.7 and ANN standard deviations larger than 1σ [*Kucera et al.*, 2005] (Figure 4e). Most of these intervals also show the highest degree of disagreement between the two techniques and so should be considered with some caution. Nevertheless, it is also the case that these no-analog situations typically occur within warm intervals, when assemblages are dominated by *G. bulloides* and *T. quinqueloba* with less than 5% of *N. pachyderma* dex., an unusual assemblage with no present-day analog in the MARGO Atlantic database (M. Kucera, personal communication, 2008). However, low *N. pachyderma* dex. abundance, even during GIs, is reported in other cores recovered from the Rockall Trough and surrounding area [e.g., *Knutz et al.*, 2007; *Kuijpers et al.*, 1998; *van Kreveld et al.*, 2000] suggesting a regional ecological feature in response to oceanographic conditions. Therefore, we consider that these SST estimates provide a generally faithful trend reconstruction, supported by the similarity of the curves to that of the GISP 2 $\delta^{18}O_{ice}$ record.

[22] MIS 3 GS-GI abrupt SST warmings average 5°C and generally vary between ~4 and ~10°C, which is consistent with the values obtained in nearby core MD01-2006 for the period between ~55.5 and ~40 ka B.P. [*Dickson et al.*, 2008] and in MIS 3-2 records further to the northwest [*van Kreveld et al.*, 2000]. The colder extreme (~4°C) is lower than coldest temperatures (~6°C) reconstructed for MIS 3 for core MD01-2461 [*Peck et al.*, 2008], likely due to latitudinal differences. Mean SSTs of ~9°C during GIs are within the range of values displayed by modern NAC in the area, GS mean values of ~5°C represent the influence of more Arctic waters [*Hansen and Østerhus*, 2000]. Remarkably, SSTs increase during MIS 2 toward the LGM (18 to 21 ka B.P.) from an initial value of ~4°C at HE 2 to ~7°–8°C at 20 ka B.P. This ~4°C to ~8°C SST oscillation displayed in the LGM fits within the SST ranges obtained in several

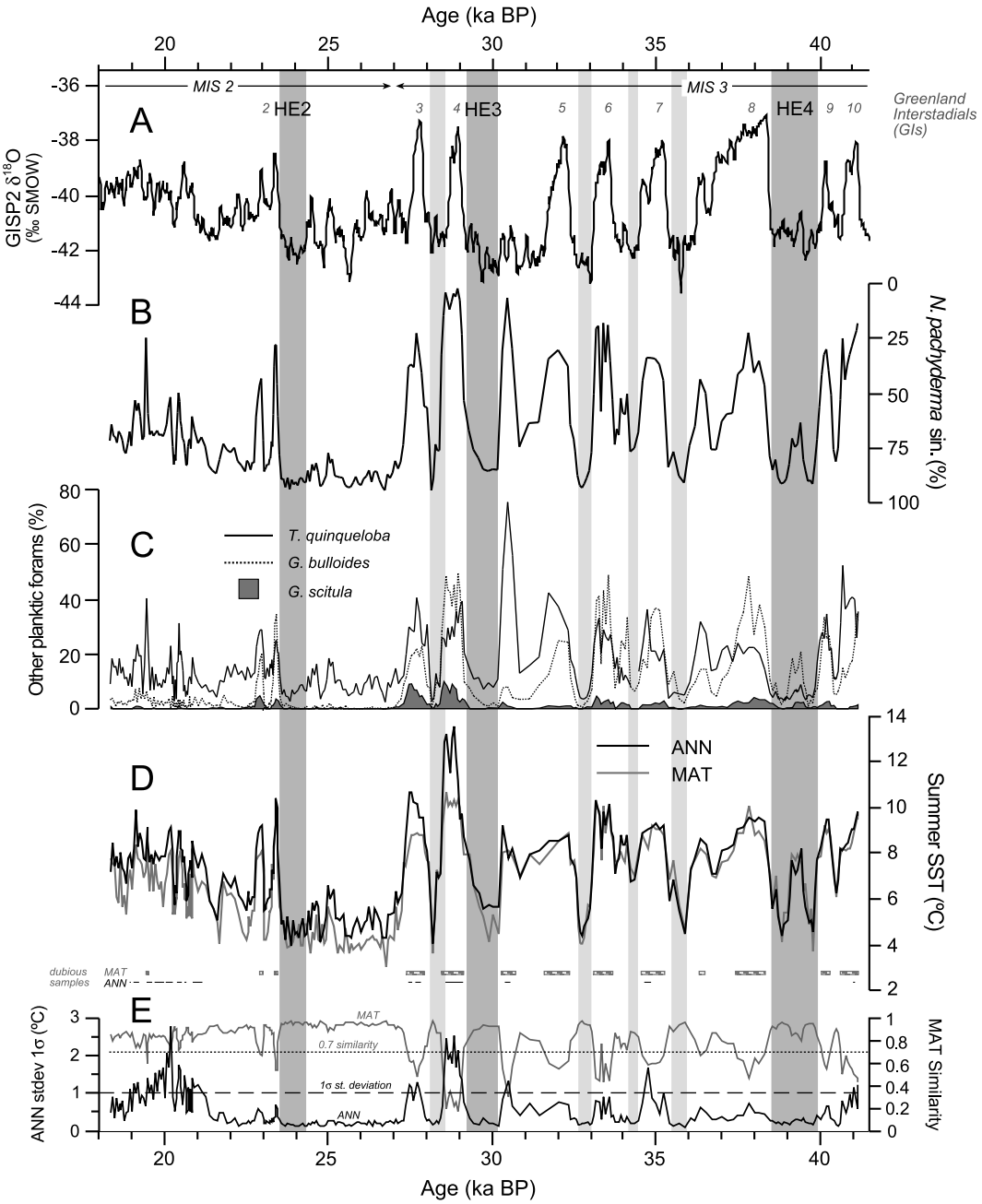

Figure 4. Planktonic foraminifera and SST records from core MD04-2829CQ. (a) GISP 2 ice core record, (b) relative abundances of *N. pachyderma* sin., (c) percent of other planktonic foraminifera taxa, (d) summer SST estimates at 10 m depth using the ANN and MAT techniques, and (e) estimated mean similarity for MAT and 1σ error for ANN. Intervals of dubious SST reconstructions are marked by small bars (MAT) and lines (ANN). Grey vertical bars mark the position of HE (dark grey) and some of the Greenland stadial (light grey) horizons.

cores south of the Iceland/Faroe Ridge for the same time interval [*Weinelt et al.*, 2003].

5.3. Lithic Composition and Abundance

[23] The flux of total IRD to the core site is continuous throughout the 41–18 ka B.P. interval (Figure 5); however warmer GIs are characterized by very low abundances of mineral grains while increased fluxes occur during HE, GSs and MIS 2. The sequence of centennial-scale IRD events superimposed on a background of increasing IRD fluxes from ~28 ka B.P. toward HE 2 is a major aspect of the record. This feature is also observed in the IRD record of cores SU90-09 and MD95-2002 [*Auffret et al.*, 2002; *Grousset et al.*, 2000, 2001] in the southeastern margin of the main IRD belt, and is similar to the increases shown in cores DAPC2 [*Knutz et al.*, 2002, 2007] and MD01-2461 [*Peck et al.*, 2006] before HE 1. Also, spectral analysis of the record (multitaper method [*Pardo-Igúzquiza*

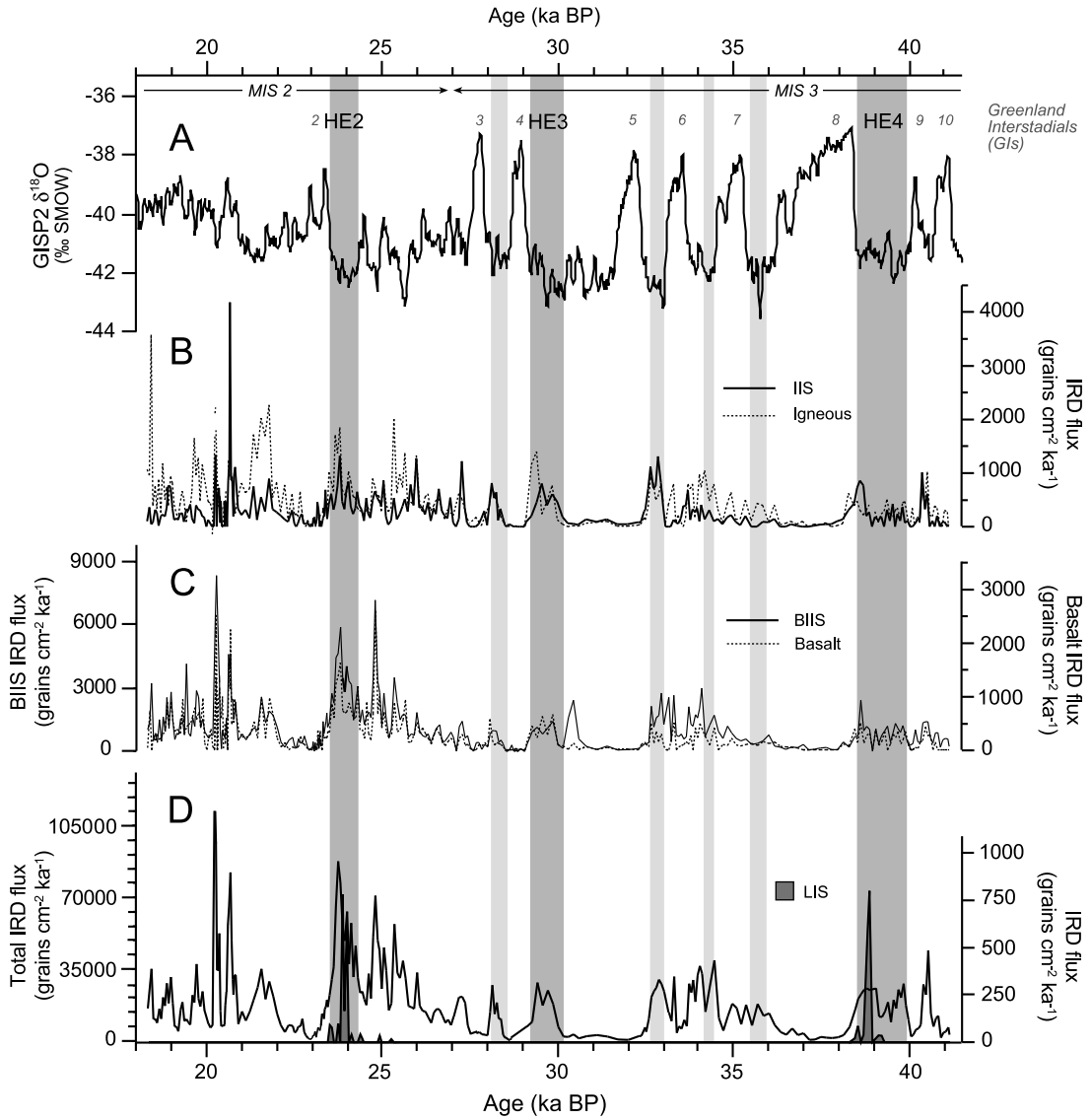

Figure 5. Correlation of the major lithic records of core MD04-2829CQ to GISP 2. (a) GISP 2 ice core record, (b and c) fluxes of the main IRD groups, and (d) total IRD and LIS-sourced cream-colored carbonate fluxes. Grey vertical bars mark HE (dark grey) and some of the Greenland stadial (light grey) horizons.

et al., 1994] with seven data tapers and spectral confidence levels located using the robust AR(1) modeling of median-smoothed spectra, not included here) shows significant centennial-scale oscillations during MIS 2, which follow a rough 500 year cyclicity, while between 30 and 41 kyr the frequency of IRD events decreases to around 1100 years.

[24] The dominant components of the mineral grain assemblage, transparent quartz and haematite-stained grains, are likely sourced in a range of locations around the North Atlantic that are impossible to isolate. The remaining grains comprise a wide range of lithologies. HE 4 and 2 stand out as peaks of finely crystalline, cream-colored carbonate (>750 grains cm^{-2} kyr^{-1} at HE 4; Figure 5d), classically diagnostic of HEs, identified as sourced from dolomitic limestones outcropping in the Hudson Bay Province of the LIS [*Andrews and Tedesco*, 1992; *Bond et al.*, 1992]. Sedimentary lithics originating from the BIIS and igneous rock fragments typically increase during cold periods. Basalt grains, petrographically similar to those described as sourced in the Tertiary Volcanic Provinces outcropping in western Scotland [*Knutz et al.*, 2007], show an abundance distribution that parallels that of the BIIS component (Figures 5b and 5c).

[25] Other volcanic grains, usually associated with the Icelandic Ice Sheet (IIS), do not show a distinct increase toward HE 2 as the other groups (Figure 5b). Some peaks could be related to tephra layers identified in other cores of this area [*Rasmussen and Thomsen*, 2004].

5.4. Hornblende Ages

[26] Hornblende grains are present throughout most of the record, although their abundance is higher at certain intervals such as HE 4 and between 26 and 23 ka B.P. (including HE 2), and 22 and 20 ka B.P. (Figure 6). A total of 419 individual grains from 184 samples covering the interval

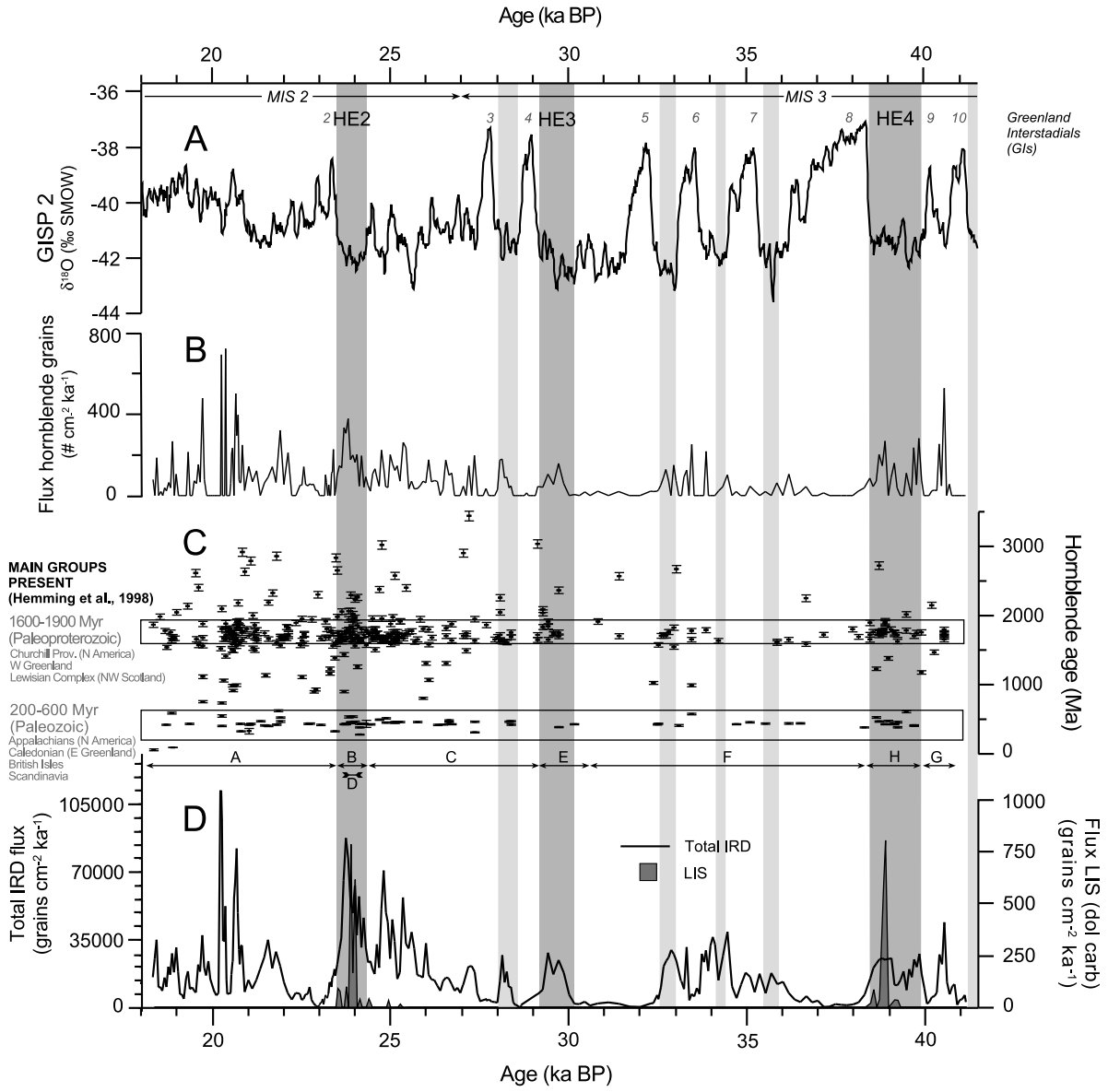

Figure 6. Comparison of (b) fluxes of horblende grains and (c) the scatterplot of measured hornblende age (in Ma) to (d) the total IRD and cream-colored carbonate grain fluxes in core MD04-2829CQ. (a) The GISP 2 oxygen isotope record is also plotted for reference. The two horizontal rectangles in the scatterplot mark Paleoproterozoic and Paleozoic grain populations, following *Hemming and Hajdas* [2003]. Arrows and letters at the bottom of the scatterplot refer to intervals in Figure 7. Grey vertical bars mark the position of HE (dark grey) and some of the Greenland stadial (light grey) horizons.

~18 to ~40 ka B.P. produced good quality Ar^{40}/Ar^{39} ages, of which 10 were discarded as grains were suspected to be pyroxenes.

[27] By dividing the sediment record into several stratigraphic intervals selected to separate HE from periods between HE (Figure 7a, <23.5 ka B.P.; Figure 7b, HE 2; Figure 7c, 24.3–29 ka B.P.; Figure 7d, cream-colored carbonate peak time span within HE 2; Figure 7e, 31–38.6 ka B.P.; Figure 7f, HE 3; Figure 7g, >40 ka B.P.; Figure 7h, HE 4) and grouping the hornblende grains accordingly, we constructed histogram graphs in order to study the population composition in each period (Figure 7). We selected the histogram age bins based on known major geological provinces around the North Atlantic [*Hemming et al.*, 1998, 2002; *Hemming and Hajdas*, 2003].

[28] The results highlight the importance of the Paleoproterozoic (1600–1900 Ma) and Paleozoic (200–600 Ma) hornblende grain populations, while the Mesoproterozoic (1400–1650 Ma) and the Early Paleoproterozoic (1900–2400 Ma) are represented by far fewer grains. The Paleoproterozoic population is dominant during most of the record, although the quantity of grains within all groups tends to vary simultaneously and the Paleozoic population is also present in high numbers during most periods. These results contrast with sediment core V23-14 from the western North Atlantic [*Hemming and Hajdas*, 2003], in where Paleopro-

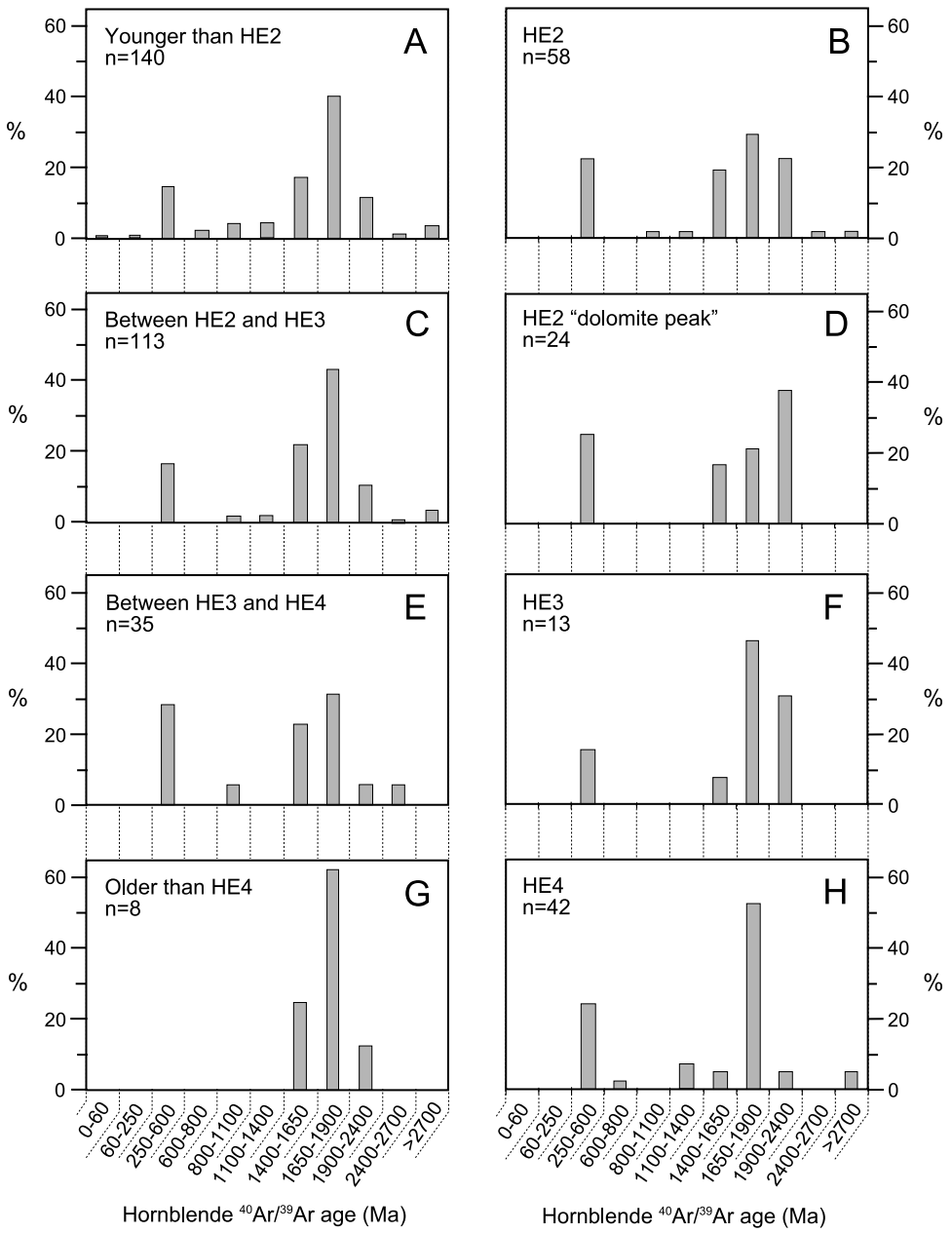

Figure 7. (a-h) Histogram plots of hornblende populations in different intervals of core MD04-2829CQ (see text and Figure 6 for interval significance). In each histogram, n is the number of hornblende grains considered for that specific age interval.

terozoic populations dominate within each HE and in the intervals between them, with far less numbers of Paleozoic (Appalachian) and Mesoproterozoic (Grenville) grains. Moreover, Paleoproterozoic grains in our core are not restricted to the intervals synchronous with the deposition of cream-colored carbonates (Figures 7d and 7h), which opposes their common apparent source in the Hudson Strait area in the Canadian Shield [*Andrews and Tedesco*, 1992; *Gwiazda et al.*, 1996; *Hemming*, 2004].

5.5. Oxygen Isotopes

[29] Structural similarity with the GS-GI cyclicity is not visible within the *G. bulloides* and *N. pachyderma* sin. $\delta^{18}O$ records in our core (Figures 8 and 9b), as also noted in other records from the region [e.g., *Lassen et al.*, 1999; *Lekens et al.*, 2006; *Rasmussen et al.*, 1996b]. Both curves show a trend of increasing $\delta^{18}O$ between HE's, attaining maximum values, indicative of coldest and/or most saline conditions, immediately before the HEs. Oxygen isotope values of *G. bulloides* remain on average 0.5‰ lighter than those of *N. pachyderma* sin., while both records converge immediately before HE 3 and 2, and during the LGM (Figure 9b).

[30] Contrary to the $\delta^{18}O$ record of *G. bulloides* the *N. pachyderma* sin. $\delta^{18}O$ record shows only small amplitude changes (~0.2‰) (Figures 8 and 9b), coincident with

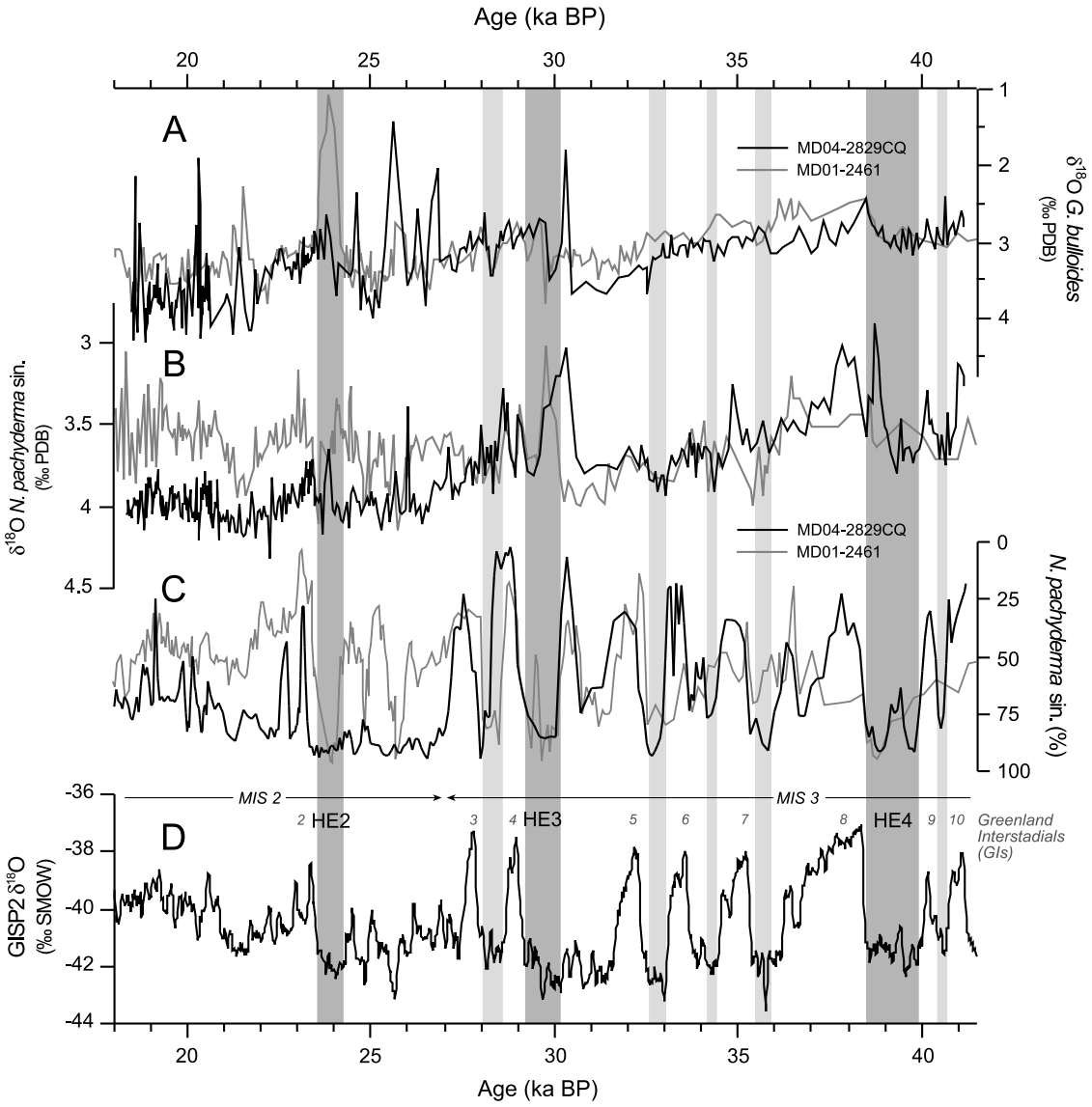

Figure 8. (a-c) Comparison of the *G. bulloides* and *N. pachyderma* sin. oxygen isotope records and the *N. pachyderma* sin. relative abundances of cores MD04-2829CQ (black lines) and MD01-2461 (grey lines). (d) The GISP 2 δ^{18}O record is included for reference. Grey vertical bars mark HE (dark grey) and some of the Greenland stadial (light grey) horizons.

the faunal and SST records. The rather higher amplitude changes along the *G. bulloides* δ^{18}O typically coincide with transient cold events and increased fluxes of IRD (Figure 9).

[31] Heinrich Events stand out in the *N. pachyderma* sin. record as isolated negative δ^{18}O anomalies of ~0.5 and ~1‰ that last 200 to 300 years at HE 2 and HE 4 respectively, and a longer ~0.75‰ reduction in δ^{18}O during HE 3 that leads the IRD event by almost 1000 years (Figure 9f). While, the HEs IRD peaks coincide with only subtle negative δ^{18}O excursions in *G. bulloides* δ^{18}O that are superimposed on a longer-term trend toward lower δ^{18}O.

[32] The short *T. quinqueloba* record (Figure 9b) seems to follow the GS-GI cyclicity, showing light peaks simultaneously to warm periods in the GISP 2 $\delta^{18}O_{ice}$ record. Similarly to the other two planktonic isotopic records, a large (~1‰) depletion characterizes the interval before the onset of HE 3.

6. Discussion

6.1. Ice Sheet Dynamics

6.1.1. Iceberg Provenance

[33] The composition of the most abundant group of IRD in core MD04-2829CQ, besides the ubiquitous quartz and haematite-stained grains (Figure 5c), has been previously associated to various outcrops in the British Isles [*Peck et al.*, 2007a; *Scourse et al.*, 2000, 2009]. The presence of soft chalk grains of Cretaceous age (C. Koch, personal communication, 2008) and of basalts, identified as originated in the Tertiary Volcanic Province of western Scotland, in the MD04-2829CQ record support this origin. Additionally,

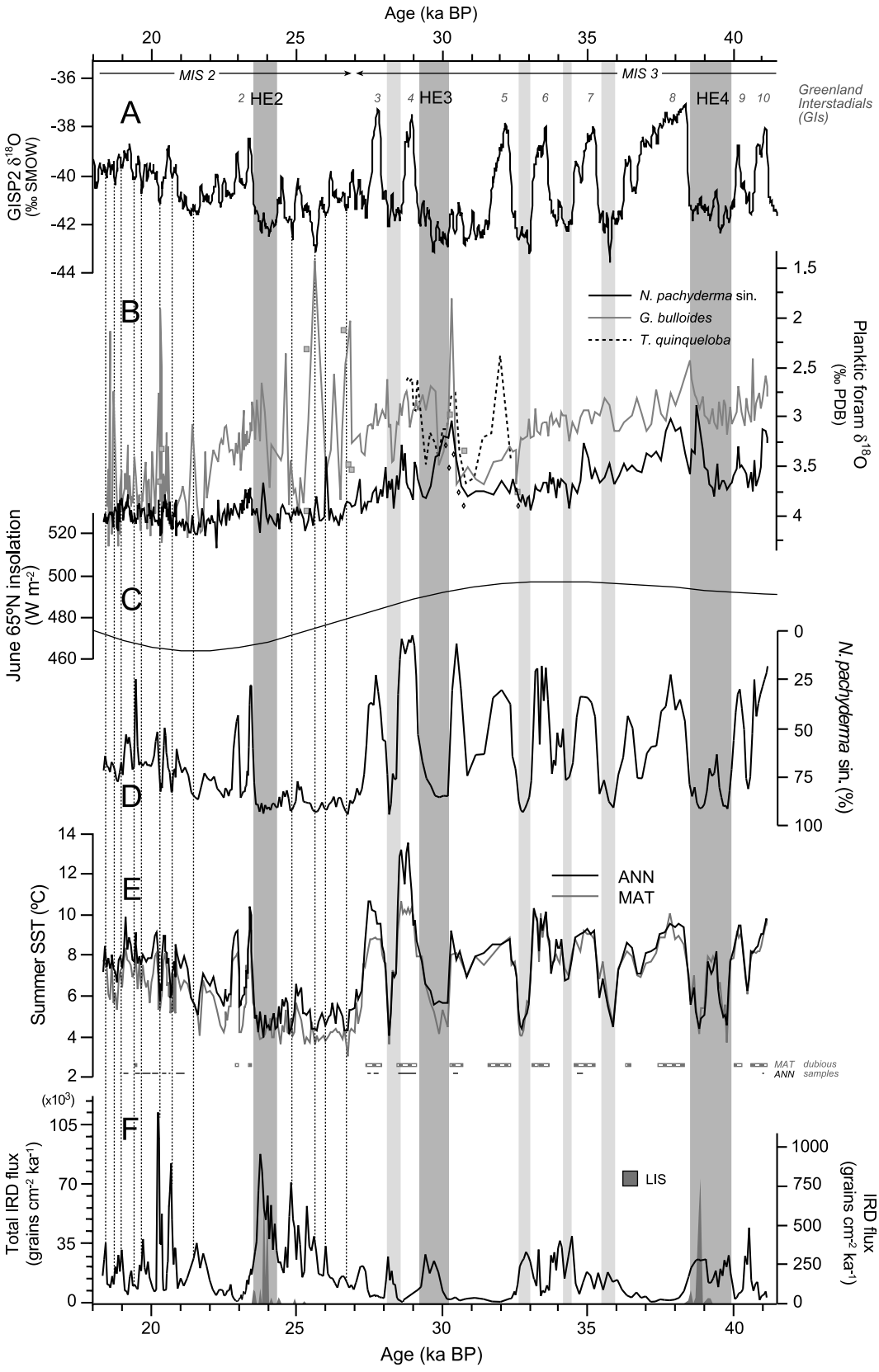
Age (ka BP)
MIS 2
MIS 3
HE2
HE3
HE4
Greenland Interstadials (GIs)
A
GISP2 δ18O (‰ SMOW)
B
N. pachyderma sin.
G. bulloides
T. quinqueloba
Planktic foram δ18O (‰ PDB)
June 65ºN insolation (W m-2)
C
D
N. pachyderma sin. (%)
E
Summer SST (ºC)
ANN
MAT
MAT dubious
ANN samples
F
Total IRD flux (grains cm-2 ka-1)
LIS
IRD flux (grains cm-2 ka-1)

Figure 9

the occurrence of occasional fine gravel sized (4–8 mm) IRD during periods of highest IRD flux points to the existence of iceberg sources within a distance of 10^1–10^2 km [*Knies et al.*, 2001; *Smith and Andrews*, 2000], consistent with the assumed expansion of BIIS margins during peak glacial conditions [*Knutz et al.*, 2001; *Sejrup et al.*, 2005]. This would also account for the sustained IRD fluxes and for the near invariable composition of IRD assemblages registered through the entire record. Alternative nearby rock fragment sources for a BIIS-like assemblage, such as the Late Paleozoic to Tertiary sediments that form the basement of the Rockall Basin within the Rockall Trough, are not considered since top layers consist mainly of recent detritic unconsolidated material [*Morewood et al.*, 2004].

[34] We also require a suitable source, or combination of sources, to explain the almost permanent flux of both Paleoproterozoic and Paleozoic hornblende grains to the core site (Figure 6). The Churchill Province units from the Hudson Strait region and the southern Labrador area are a likely origin for both populations [*Gwiazda et al.*, 1996; *Hemming et al.*, 1998, 2002; *Hemming*, 2004]. However, LIS-sourced, cream-colored carbonates are only present at transient (200–300 years) episodes within the GSs that contain HE 2 and HE 4 (Figures 5d and 9f). These intervals correlate to geochemical and magnetic evidence from other northeast Atlantic cores [*Grousset et al.*, 2000; *Peck et al.*, 2007a; *Peters et al.*, 2008], which show that the influence of the LIS signal in the northeast Atlantic is exclusive to those horizons. Thus, while it is possible that the Paleoproterozoic and Paleozoic hornblende population at those events may have been mostly or entirely sourced in the LIS, lack of further evidence of a LIS imprint in our core during non-HS intervals suggests that other sources of Paleoproterozoic and Paleozoic hornblende grains were also contributing. Those other potential areas include Greenland and the Lewisian Complex outcropping in the Outer Hebrides (northwest Scotland) for the Paleoproterozoic, and Scandinavia and the British Isles for the Paleozoic. The Lewisian Complex seems the most probable source of Paleoproterozoic grains due to its proximity and to the documented flow path of ice streams of the northwestern BIIS margin [*Sejrup et al.*, 2005] (Figure 1). It is also notable that the interval of highest concentration of Paleoproterozoic hornblende grains (Figure 6) is simultaneous to the steady increase in the IRD fluxes and the centennial-scale events in the period 27–20 ka B.P., documented as the interval of BIIS advance to the shelf break [*Wilson and Austin*, 2002], supporting a West Scotland origin for most Paleoproterozoic hornblende grains. A northeastern Atlantic source such as Scandinavia and the British Isles is also more likely for the Paleozoic population of our core, since grains of this age range are more common in the Nordic Seas [*Hemming et al.*, 2002]. This likely explains the differences in hornblende distributions from our core (Figure 7) to those of core VM23-14 in the Central North Atlantic [*Hemming and Hajdas*, 2003] in where Paleozoic populations are not as important.

6.1.2. BIIS Evolution

[35] The frequency and scale of iceberg discharge events recorded in core MD04-2829CQ are likely connected to BIIS ice volume and its growth throughout the last glacial period. The smaller, millennial-scale discharges of roughly equal magnitude during MIS 3–related cold events contrast with the increasingly larger, centennial-scale IRD peaks dominating MIS 2 (Figures 5d and 9f), and indicate substantial changes in the extent of nearby BIIS and the development of fringing marine ice shelves, as suggested by *Scourse et al.* [2009]. Land-based evidence from Scotland shows an interstadial period between 38.1 and 32 ka B.P. (the Alesund/Denekamp/Sadnes interstadial), widely recognized in Western Europe and equivalent in age to GIs 8 to 5 [*Whittington and Hall*, 2002]. This warmer period was followed in land by major climate deterioration and ice advance to the west and south after ~32 ka B.P. [*Brown et al.*, 2007; *Finlayson et al.*, 2010]. In the marine record, a combination of enhanced NWEIS build-up rate and general sea level lowering due to decreasing insolation from ~28 ka B.P. seems the probable cause of this shift in the frequency of iceberg calving from that point. Both circumstances apparently triggered continuous centennial-scale readjustments of the extended marine-based NWEIS margins during this younger period, also evidenced in nearby sediment records off northeast Europe and Iceland [*Fronval et al.*, 1995; *Knutz et al.*, 2007; *Lassen et al.*, 1999; *Lekens et al.*, 2006; *Peck et al.*, 2006; *Rasmussen et al.*, 1996a; *Scourse et al.*, 2009; *van Kreveld et al.*, 2000], which are all consistent with short-term cooling episodes in Greenland. This high-frequency response is also observed prior to HE 1 [*Knutz et al.*, 2007; *Peck et al.*, 2006]. *Knutz et al.* [2007] suggest that increasing 65°N summer insolation following the LGM was a potential triggering mechanism for the centennial IRD cycles observed in core DAPC2 showing early BIIS disintegration prior to HE 1. Our data from core MD04-2829CQ indicate that both increasing and decreasing 65°N summer insolation are associated with similar readjustments in the BIIS margins and point to a sustained metastability of the BIIS throughout MIS 2.

[36] The absence of large peaks in the total IRD flux for HE 3 and HE 4 in core MD04-2829CQ, reflecting the relatively small size of the BIIS during MIS 3, contrasts with those of records inside the main IRD belt between 40 and 55°N [after *Ruddiman*, 1977; *Hemming*, 2004], in which HEs represent the most important discharge episodes [*Bond et al.*, 1993; *Bond and Lotti*, 1995]. LIS-sourced IRD accumulation during HE 2 and HE 4 decreases toward the northeast North Atlantic and outside this belt, and is also supported by smaller fluxes of LIS-sourced cream-colored carbonates at Rosemary Bank in contrast to those from core MD01-2461 in the Porcupine Bight, offshore southwest

Figure 9. Compilation of some of the records obtained for core MD04-2829CQ: (b) surface (*G. bulloides* and *T. quinqueloba*) and subsurface (*N. pachyderma* sin.) oxygen isotopes (with extra *N. pachyderma* sin. and *G. bulloides* samples in open rhombi and grey squares, respectively; explanation in the text), (d) *N. pachyderma* sin. relative abundances, and (e) summer SST estimates at 10 m depth as in Figure 4e, and (f) total IRD and LIS-sourced cream-colored carbonate fluxes. (a) The GISP 2 oxygen isotope record and (c) the June 65°N mean insolation are plotted for reference. Grey vertical bars mark the position of HE (dark grey) and some of the Greenland stadial (light grey) horizons.

Ireland [*Peck et al.*, 2006], and of ODP Site 609 and core VE23-81 further offshore on the west flank of the Rockall Trough [*Bond and Lotti*, 1995]. These decreasing flux gradients indicate that the LIS only played a fairly minor role in IRD accumulation at Rosemary Bank that was limited to short intervals within HE 4 and HE 2. Recent data on mineral magnetic measurements from core MD95-2006 recovered from the nearby Barra Fan [*Peters et al.*, 2008] support this interpretation.

6.2. Ice Sheet–Upper Ocean Connection

[37] Today *N. pachyderma* sin. thrives in the Nordic Sea and Arctic Ocean at the base of the summer seasonal surface mixed layer at ~50 m [*Bauch et al.*, 1997; *Jonkers et al.*, 2010]. In the subpolar North Atlantic, *G. bulloides* calcifies within 0–60 m water depth, blooming in the summer months [*Cortijo et al.*, 1997; *Ganssen and Kroon*, 2000]. Field and modeling evidence from present-day and LGM assemblages in polar and subpolar regions [*Fraile et al.*, 2009a, 2009b; *Jonkers et al.*, 2010; *Kohfeld et al.*, 1996] suggest that glacial blooms of both *G. bulloides* and of *N. pachyderma* sin. occurred during the summer months. However, given the habitat preferences of the two species we can interpret the *G. bulloides* δ^{18}O record as being a summer SST signal and *N pachyderma* sin. δ^{18}O as representing mean annual subsurface conditions [*Peck et al.*, 2008]. The ~0.5‰ offset between both δ^{18}O records at this site prior to the LGM (Figure 9b) points to a strong gradient between surface and subsurface waters during the summer months, with denser (cooler and/or saltier) waters below lighter (warmer/less saline) surface waters. At the LGM the two δ^{18}O records converge suggesting that both species are living in the same water mass, suggestive of year-round mixing of the upper waters/no seasonal thermocline.

[38] A comparison of both isotopic records with the equivalent from core MD01-2461 in the Porcupine Seabight (SW Ireland) [*Peck et al.*, 2006] (Figure 8) reveals clear similarities in upper water column structure at the two sites. The surface isotopic signals seem to represent roughly equivalent water masses at both locations. Since *G. bulloides* from the LGM seem to calcify in summer in both areas [*Fraile et al.*, 2009b], the small occasional difference between both records can be interpreted as a minor latitudinal temperature gradient and/or meltwater lenses.

[39] Comparable *N. pachyderma* sin. δ^{18}O records from the two sites suggest similar subsurface water mass properties at both locations up until ~27 ka B.P. After this time, the δ^{18}O *N. pachyderma* sin. record at the more southerly site becomes up to 0.5‰ lighter than in Rosemary Bank, evidencing clear differences between both records.

[40] A likely explanation for the different behavior of both records from ~27 ka B.P. relies in the migration of the Polar Front. The comparison of *N. pachyderma* sin. relative abundance records (Figure 8) during MIS 3 shows near synchronous variations between both sites until ~27 ka B.P., allowing us to infer an unstable Polar Front migrating rapidly along the western BIIS margin, across both sites, simultaneously to GS-GI cyclicity. Additional evidence of the migration of the Polar Front as far south as 40°N during HE and some of the GS is observed in records from the western Iberian Margin [*Eynaud et al.*, 2009; *Salgueiro et al.*, 2010; *Voelker et al.*, 2009]. In contrast, at the onset of MIS 2 the persistent dominance of *N. pachyderma* sin. in the faunal assemblage and heavier δ^{18}O values at Rosemary Bank are consistent with a scenario of BIIS build-up and a likely almost stable position of the Polar Front south of core MD04-2829CQ. Periodic migration of the Polar Front south of MD01-2461 is reflected in our records by the convergence of both isotopic and faunal signals, at 25.7 ka B.P., 25 ka B.P. and HE 2. After HE 2 the Polar Front remains between the two sites but appears to periodically retreat north of core MD04-2829CQ when *N. pachyderma* sin. relative abundance from this site decreases to converge with MD01-2461, although this is not expressed in the isotopic records. BIIS advance at ~21.5 ka B.P. (also observed by *Knutz et al.* [2007] and *Peck et al.* [2006]) is associated with a final advance of the Polar Front toward MD01-2461, while three further Polar Front retreats northward of Rosemary Bank are noted at 20.1, 19.9 and 19 ka B.P.

[41] Cold events such as the ones at ~25.7 and ~21.5 ka B.P. produced meltwater plumes both north and south of the BIIS, as reflected in the light δ^{18}O peaks in *G. bulloides* recorded at both sites. At HE 2, the amount of melt waters and icebergs seems to be much larger at the southern front of the BIIS, as shown by the large isotopic spike and IRD flux recorded in core MD01-2461 (Figure 8) [*Peck et al.*, 2007a] and in core MD95-2002 further southeast along the continental margin [*Grousset et al.*, 2000; *Auffret et al.*, 2002].

[42] Contrary to the *N. pachyderma* sin. record, the small response of *G. bulloides* to the events recorded during HE 2 and MIS 2 in core MD04-2829CQ likely show a partially biased record affected by the harsh conditions of average years, with low to very low abundances (Figure 4) and/or summer blooming restricted to the warmer years.

[43] Isotopic data from core MD04-2829CQ suggest that MIS 3 GS conditions were characterized by cooling synchronously to iceberg calving from the BIIS (Figure 9b). The frequency and scale of iceberg discharge events and hence the input of low-salinity waters to the surface layers water are greatly enhanced after ~31 ka B.P. as may be inferred from the increased magnitude of the light *G. bulloides* δ^{18}O excursions and of simultaneous maxima in IRD flux during the centennial-scale BIIS-sourced events prior to HE 2 and during the LGM. The absence or significantly smaller scale of the related decreases in the *N. pachyderma* sin. δ^{18}O record during most of these cold intervals is remarkable since the associated IRD flux peaks are of similar or even greater magnitude to those recorded during HE 3 and 4. This may reflect a stronger water column stratification resulting in the migration of *N. pachyderma* sin. to deeper depths below the halocline [*Kohfeld et al.*, 1996]. Alternatively, *Elliot et al.* [1998] attributed an analogous *N. pachyderma* sin. δ^{18}O signal to a combination of decreased meltwater flux and its origin in coastal ice sheets, therefore showing a less fractionated isotopic signature. However, since the BIIS is in all cases the likely source of meltwater and the ice sheet size was far larger after ~28 ka B.P. than during MIS 3, the degree of distance-based isotopic fractionation between ice accumulation areas and the ice sheet margins should have increased rather than decreased as the BIIS increased its ice volume, and for

the interval before ~28 ka B.P. the relatively low fractionation may have reduced the meltwater signal recorded in the *N. pachyderma* sin. δ^{18}O. The magnitude of the *G. bulloides* δ^{18}O light anomalies and IRD fluxes between 28 and 18 ka B.P. in MD04-2829CQ suggest that a meltwater lens may have been a persistent feature at that time/site, although, because of the low abundances of *G. bulloides*, this interpretation should be treated with some caution. Overall, it seems probable that the freshening associated with the BIIS IRD surging only influenced the surface waters and did not fully affect deeper layers. The scale of some of these calving events (such as those at ~25.7 ka B.P. and ~21.5 ka B.P.) must have involved much of the western margin of the BIIS since simultaneous meltwater plumes were also recorded in core MD01-2461 (Figure 8). Larger fluxes of IRD at MD01-2461 during these two events [*Peck et al.*, 2007a] compared with our core further north may be indicative of higher instability in the southwestern BIIS margin at those times.

[44] As highlighted in Figure 9 it is evident that in our core HE 4 and 2 are characterized by prominent light peaks in the isotopic record of *N. pachyderma* sin. coincident with the arrival of LIS-sourced material. These excursions are not accompanied by large depletions of the isotopic values of *G. bulloides* as during centennial-scale cooling events; rather, negative values in *G. bulloides* δ^{18}O are less clearly defined, and tend to lag those of *N. pachyderma* sin. It has been suggested that convergence of surface and subsurface δ^{18}O values during HE represents strong mixing of the upper water column down to ~100–200 m [*Simstich et al.*, 2003], and a recent study suggest that this deepening of the surface mixed layer might have been caused by a brief increase in storminess during GSs containing HEs [*Rashid and Boyle*, 2007]. However, convergence of our isotopic records is not evident in HE 4 and HE 2 and only HE 3 shows possible evidence of this process although leading the maximum IRD flux by a few hundreds of years.

[45] HE 3 stands out in our record as a distinct event due to the absence of LIS-sourced material and to the particular isotopic signals recorded in this interval. Before this event and for a ~500 year interval, δ^{18}O values from three different species representing diverse depths in the upper water masses decrease simultaneously (Figure 9b). A prominent negative anomaly is also observed in the *N. pachyderma* sin. δ^{18}O record at MD01-2461 around the same time (Figure 8), with an associated increase in benthic δ^{18}O and decrease in benthic δ^{13}C values and ^{14}C marine reservoir ages [*Peck et al.*, 2006, 2007b]. We note that these anomalies coincide with extremely low IRD fluxes at MD04-2829CQ (Figure 9f), consisting predominantly of mica flakes, and of a faunal assemblage dominated almost entirely by *T. quinqueloba* in the planktonic foraminiferal fraction (Figure 4). Together, all these indicators seem to show either the presence of an exceptionally warm or less saline water mass apparently unconnected to BIIS calving events, since its IRD composition is unique. This event can be correlated to the so-called "DO 4.1" in Greenland and Antarctica ice core records [*EPICA Community Members*, 2006] and represents a warming phase in those records and in the Western Mediterranean [*Sierro et al.*, 2009]. Warming is not obvious from our records as *T. quinqueloba* is characterized as an extremely resistant species that can survive to very low salinity conditions [*Simstich et al.*, 2003], and has been previously interpreted as a marker for the position of the Arctic front [*Johannessen et al.*, 1994; *Eynaud et al.*, 2009]. Moreover, simultaneously to our event *Lekens et al.* [2006] registered a "low salinity" event focused in the southern Nordic Seas apparently caused by the breakage of ice dams and flooding of freshwater glacial lakes from the North Sea. These authors consider this low δ^{18}O as representing HE 3 in this area, but our records indicate that, if being the same event, it precedes HE 3 itself (or at least BIIS IRD response to HE 3) by 2–3 centuries, in line with the observations by *van Kreveld et al.* [2000] in the Irminger Sea.

7. Conclusions

[46] This study emphasizes the high sensitivity of the BIIS as an important component of the climate system of the Last Glacial in the North Atlantic. The interval between 41 and 18 ka B.P. was characterized in the Northeast Atlantic by a succession of iceberg calving events sourced in the BIIS synchronous with decreases in SSTs that reflect the southern advances of the Polar Front. Those events occurred with millennial frequencies from 41 to 28 ka B.P. when the BIIS was not fully developed, and at centennial timescales from 28 to 18 ka B.P. reflecting the ice sheet building up and simultaneous and rapid development of fringing marine ice shelve margins, resulting in characteristic metastability. The data confirm the strong coupling between BIIS instabilities and surface ocean circulation during MIS 3/2, and demonstrate BIIS ability to modify the North Atlantic Current on its flow toward the Nordic Seas; petrological evidence indicates a superimposed contribution of the LIS during HE 2 and 4.

[47] **Acknowledgments.** We thank Julia Becker for stable isotope analysis and advice, Helen Medley for guidance in laboratory work, and Millie Mendelson (LDEO) for assistance in AMS sample picking. Constructive comments by Antje Voelker and an anonymous reviewer helped to improve the manuscript. The work was supported by the U.K. National Environmental Research Council (NERC). Radiocarbon dating was carried out by the NERC Radiocarbon Laboratory. R.Z. acknowledges funding by the MEC, Spain, through grant CGL2007-61579/CLI.

References

Andrews, J. T., and K. Tedesco (1992), Detrital carbonate-rich sediments, northwestern Labrador Sea: Implications for ice-sheet dynamics and iceberg rafting (Heinrich) events in the North Atlantic, *Geology*, *20*, 1087–1090, doi:10.1130/0091-7613(1992)020<1087:DCRSNL>2.3.CO;2.

Auffret, G., S. Zaragosi, B. Dennielou, E. Cortijo, D. Van Rooij, F. Grousset, C. Pujol, F. Eynaud, and M. Siegert (2002), Terrigenous fluxes at the Celtic margin during the last glacial cycle, *Mar. Geol.*, *188*, 79–108, doi:10.1016/S0025-3227(02)00276-1.

Austin, W. E. N., E. Bard, J. B. Hunt, D. Kroon, and J. D. Peacock (1995), The ^{14}C age of the Icelandic Vedde Ash: Implications for Younger Dryas marine reservoir age corrections, *Radiocarbon*, *37*, 53–62.

Bard, E. (1988), Correction of accelerator mass spectrometry ^{14}C ages measured in planktonic foraminifera: Paleoceanographic implications, *Paleoceanography*, *3*, 635–645, doi:10.1029/PA003i006p00635.

Bard, E., M. Arnold, J. Duprat, J. Moyes, and J.-C. Duplessy (1987), Bioturbation effects on abrupt climatic changes recorded in deep sea sediments. Correlation between d18O profiles and accelerator 14C dating, in *Abrupt Climatic Change*, edited by W. H. Berger and L. D. Labeyrie, pp. 263–278, D. Reidel, Dordrecht, Netherlands.

Bard, E., M. Arnold, J. Mangerud, M. Paterne, L. Labeyrie, J. Duprat, M. A. Melieres, E. Sonstegaard, and J. C. Duplessy (1994), The North Atlantic atmosphere-sea surface ^{14}C gradient during the Younger Dryas

climatic event, *Earth Planet. Sci. Lett.*, *126*, 275–287, doi:10.1016/0012-821X(94)90112-0.

Bauch, D., J. Carstens, and G. Wefer (1997), Oxygen isotope composition of living *Neogloboquadrina pachyderma* (sin) in the Arctic Ocean, *Earth Planet. Sci. Lett.*, *146*, 47–58, doi:10.1016/S0012-821X(96)00211-7.

Bé, A. W. H. (1977), An ecological, zoogeographic and taxonomic review of recent planktonic foraminifera, in *Oceanic Micropaleontology*, edited by A. T. S. Ramsay, pp. 1–100, Academic, London.

Bigg, G. R., R. Levine, C. D. Clark, S. L. Greenwood, H. Haflidason, A. L. C. Hughes, A. Nygård, and H. P. Sejrup (2010), Last glacial ice-rafted debris off southwestern Europe: The role of the British-Irish Ice Sheet, *J. Quat. Sci.*, *25*, 689–699, doi:10.1002/jqs.1345.

Bond, G. C., and R. Lotti (1995), Iceberg discharges into the North Atlantic on millennial time scales during the last glaciation, *Science*, *267*, 1005–1010 doi:10.1126/science.267.5200.1005.

Bond, G., et al. (1992), Evidence for massive discharges of icebergs into the North Atlantic ocean during the last glacial period, *Nature*, *360*, 245–249, doi:10.1038/360245a0.

Bond, G., W. Broecker, S. Johnsen, J. McManus, L. Labeyrie, J. Jouzel, and G. Bonani (1993), Correlations between climatic records from North Atlantic sediments and Greenland ice, *Nature*, *365*, 143–147, doi:10.1038/365143a0.

Brown, E. J., J. Rose, R. G. Coope, and J. J. Lowe (2007), An MIS 3 age organic deposits from Balglass Burn, central Scotland: Palaeoenvironmental significance and implications for the timing of the onset of the LGM ice sheet in the vicinity of the British Isles, *J. Quat. Sci.*, *22*, 295–308, doi:10.1002/jqs.1028.

Butzin, M., M. Prange, and G. Lohmann (2005), Radiocarbon simulations for the glacial ocean: The effects of wind stress, Southern Ocean sea ice and Heinrich events, *Earth Planet. Sci. Lett.*, *235*, 45–61, doi:10.1016/j.epsl.2005.03.003.

Cao, L., R. G. Fairbanks, R. A. Mortlock, and M. J. Risk (2007), Radiocarbon reservoir age of high latitude North Atlantic surface water during the last deglacial, *Quat. Sci. Rev.*, *26*, 732–742, doi:10.1016/j.quascirev.2006.10.001.

Cortijo, E., L. Labeyrie, L. Vidal, M. Vautravers, M. Chapman, J. C. Duplessy, M. Elliot, M. Arnold, J. L. Turon, and G. Auffret (1997), Changes in sea surface hydrology associated with Heinrich event 4 in the North Atlantic Ocean between 40° and 60°N, *Earth Planet. Sci. Lett.*, *146*, 29–45, doi:10.1016/S0012-821X(96)00217-8.

Dansgaard, W., et al. (1993), Evidence for general instability of past climate from a 250-kyr ice-core record, *Nature*, *364*, 218–220, doi:10.1038/364218a0.

Dickson, A. J., W. E. N. Austin, I. R. Hall, M. A. Maslin, and M. Kucera (2008), Centennial-scale evolution of Dansgaard-Oeschger events in the northeast Atlantic Ocean between 39.5 and 56.5 ka B.P., *Paleoceanography*, *23*, PA3206, doi:10.1029/2008PA001595.

Elliot, M., L. Labeyrie, G. Bond, E. Cortijo, J. L. Turon, N. Tisnerat, and J. C. Duplessy (1998), Millennial-scale iceberg discharges in the Irminger Basin during the last glacial period: Relationship with the Heinrich events and environmental settings, *Paleoceanography*, *13*, 433–446, doi:10.1029/98PA01792.

EPICA Community Members (2006), One-to-one coupling of glacial climate variability in Greenland and Antarctica, *Nature*, *444*, 195–198, doi:10.1038/nature05301.

Eynaud, F., et al. (2009), Position of the Polar Front along the western Iberian margin during key cold episodes of the last 45 ka, *Geochem. Geophys. Geosyst.*, *10*, Q07U05, doi:10.1029/2009GC002398.

Fairbanks, R. G., R. A. Mortlock, T.-C. Chiu, L. Cao, A. Kaplan, T. P. Guilderson, T. W. Fairbanks, A. L. Bloom, P. M. Grootes, and M.-J. Nadeau (2005), Radiocarbon calibration curve spanning 0 to 50,000 years BP based on paired $^{230}Th/^{234}U$ and ^{14}C dates on pristine corals, *Quat. Sci. Rev.*, *24*, 1781–1796, doi:10.1016/j.quascirev.2005.04.007.

Finlayson, A., J. Merritt, M. Browne, J. Merritt, A. McMillan, and K. Whitbread (2010), Ice sheet advance, dynamics, and decay configurations: Evidence from west central Scotland, *Quat. Sci. Rev.*, *29*, 969–988, doi:10.1016/j.quascirev.2009.12.016.

Fraile, I., S. Mulitza, and M. Schulz (2009a), Modeling planktonic foraminiferal seasonality: Implications for sea-surface temperature reconstructions, *Mar. Micropaleontol.*, *72*, 1–9, doi:10.1016/j.marmicro.2009.01.003.

Fraile, I., M. Schulz, S. Mulitza, U. Merkel, M. Prange, and A. Paul (2009b), Modeling the seasonal distribution of planktonic foraminifera during the Last Glacial Maximum, *Paleoceanography*, *24*, PA2216, doi:10.1029/2008PA001686.

Fronval, T., E. Jansen, J. Bloemendal, and S. Johnsen (1995), Oceanic evidence for coherent fluctuations in Fennoscandian and Laurentide ice sheets on millennium timescales, *Nature*, *374*, 443–446, doi:10.1038/374443a0.

Ganssen, G., and D. Kroon (2000), The isotopic signature of planktonic foraminifera from NE Atlantic surface sediments: Implications for the reconstruction of past oceanic conditions, *J. Geol. Soc.*, *157*, 693–699, doi:10.1144/jgs.157.3.693.

Greenland Ice Core Project Members (1993), Climate instability during the last interglacial period recorded in the GRIP ice core, *Nature*, *362*, 203–207.

Grootes, P. M., and M. Stuiver (1997), Oxygen 18/16 variability in Greenland snow and ice with 10^{-3}– to 10^{5}-year time resolution, *J. Geophys. Res.*, *102*, 26,455–26,470, doi:10.1029/97JC00880.

Grootes, P. M., M. Stuiver, J. W. C. White, S. Johnsen, and J. Jouzel (1993), Comparison of the oxygen isotope records from the GISP 2 and GRIP Greenland ice cores, *Nature*, *366*, 552–554, doi:10.1038/366552a0.

Grousset, F. E., C. Pujol, L. Labeyrie, G. Auffret, and A. Boelaert (2000), Were the North Atlantic Heinrich events triggered by the behavior of the European ice sheets?, *Geology*, *28*, 123–126, doi:10.1130/0091-7613(2000)28<123:WTNAHE>2.0.CO;2.

Grousset, F. E., E. Cortijo, S. Huon, L. Herve, T. Richter, D. Burdloff, J. Duprat, and O. Weber (2001), Zooming in on Heinrich layers, *Paleoceanography*, *16*, 240–259, doi:10.1029/2000PA000559.

Gwiazda, R. H., S. R. Hemming, and W. S. Broecker (1996), Tracking the sources of icebergs with lead isotopes: The provenance of ice-rafted debris in Heinrich layer 2, *Paleoceanography*, *11*, 77–93, doi:10.1029/95PA03135.

Haapaniemi, A. I., et al. (2010), Source, timing, frequency and flux of ice-rafted detritus to the Northeast Atlantic margin, 30–12 ka: Testing the Heinrich precursor hypothesis, *Boreas*, *39*(3), 576–591.

Hall, I. R., and J. Scourse (2005), *Sequencing Ocean-Ice Interaction, MD141 Cruise Report, report*, 20 pp., Cardiff Univ., Cardiff, U. K.

Hall, I. R., S. B. Moran, R. Zahn, P. C. Knutz, C.-C. Shen, and R. L. Edwards (2006), Accelerated drawdown of meridional overturning in the late-glacial Atlantic triggered by transient pre-H event freshwater perturbation, *Geophys. Res. Lett.*, *33*, L16616, doi:10.1029/2006GL026239.

Hansen, B., and S. Østerhus (2000), North Atlantic-Nordic Seas exchanges, *Prog. Oceanogr.*, *45*, 109–208, doi:10.1016/S0079-6611(99)00052-X.

Hemming, S. R. (2004), Heinrich Events: Massive late Pleistocene detritus layers of the North Atlantic and their global climate imprint, *Rev. Geophys.*, *42*, RG1005, doi:10.1029/2003RG000128.

Hemming, S. R., and I. Hajdas (2003), Ice-rafted detritus evidence from $^{40}Ar/^{39}Ar$ ages of individual hornblende grains for evolution of the eastern margin of the Laurentide ice sheet since 43 ^{14}C ky, *Quat. Int.*, *99–100*, 29–43, doi:10.1016/S1040-6182(02)00110-6.

Hemming, S. R., W. S. Broecker, W. D. Sharp, G. C. Bond, R. H. Gwiazda, J. F. McManus, M. Klas, and I. Hajdas (1998), Provenance of Heinrich layers in core V28–82, northeastern Atlantic: $^{40}Ar/^{39}Ar$ ages of ice-rafted hornblende, Pb isotopes in feldspar grains, and Nd-Sr-Pb isotopes in the fine sediment fraction, *Earth Planet. Sci. Lett.*, *164*, 317–333, doi:10.1016/S0012-821X(98)00224-6.

Hemming, S. R., C. M. Hall, P. E. Biscaye, S. M. Higgins, G. C. Bond, J. F. McManus, D. C. Barber, J. T. Andrews, and W. S. Broecker (2002), $^{40}Ar/^{39}Ar$ ages and $^{40}Ar^*$ concentrations of fine-grained sediment fractions from North Atlantic Heinrich layers, *Chem. Geol.*, *182*, 583–603, doi:10.1016/S0009-2541(01)00342-4.

Hibbert, F. D., W. E. N. Austin, M. J. Leng, and R. W. Gatliff (2010), British Ice Sheet dynamics inferred from North Atlantic ice-rafted debris records spanning the last 175 000 years, *J. Quat. Sci.*, *25*, 461–482, doi:10.1002/jqs.1331.

Hodell, D. A., and J. H. Curtis (2008), Oxygen and carbon isotopes of detrital carbonate in North Atlantic Heinrich Events, *Mar. Geol.*, *256*, 30–35, doi:10.1016/j.margeo.2008.09.010.

Johannessen, T., E. Jansen, A. Flatøy, and A. C. Ravelo (1994), The relationship between surface water masses, oceanographic fronts and paleoclimatic proxies in surface sediments of the Greenland, Iceland, Norwegian Seas, in *Carbon Cycling in the Glacial Ocean*, *NATO ASI Ser., Ser. I*, pp. 61–86, Springer, Berlin.

Jonkers, L., G. J. A. Brummer, F. J. C. Peeters, H. M. Van Aken, and F. De Jong (2010), Seasonal stratification, shell flux, and oxygen isotope dynamics of left-coiling *N. pachyderma* and *T. quinqueloba* in the western subpolar North Atlantic, *Paleoceanography*, *25*, PA2204, doi:10.1029/2009PA001849.

Keigwin, L. D., and S. J. Lehman (1994), Deep circulation change linked to Heinrich Event-1 and Younger Dryas in a mid-depth North Atlantic core, *Paleoceanography*, *9*, 185–194, doi:10.1029/94PA00032.

Kennett, J. P., and M. S. Srinivasan (1983), *Neogene Planktonic Foraminifera: A Phylogenetic Atlas*, 230 pp., Hutchinson Ross, Stroudsburg, Pa.

Knies, J., H. P. Kleiber, J. Matthiessen, C. Müller, and N. Nowaczyk (2001), Marine ice-rafted debris records constrain maximum extent of Saalian and Weichselian ice-sheets along the northern Eurasian

margin, *Global Planet. Change*, *31*, 45–64, doi:10.1016/S0921-8181(01)00112-6.

Knutz, P. C., W. E. N. Austin, and E. J. W. Jones (2001), Millennial-scale depositional cycles related to British Ice Sheet variability and North Atlantic paleocirculation since 45 kyr B.P., Barra Fan, U.K. margin, *Paleoceanography*, *16*, 53–64, doi:10.1029/1999PA000483.

Knutz, P. C., I. R. Hall, R. Zahn, T. L. Rasmussen, A. Kuijpers, M. Moros, and N. J. Shackleton (2002), Multidecadal ocean variablity and NW European ice sheet surges during the last deglaciation, *Geochem. Geophys. Geosyst.*, *3*(12), 1077, doi:10.1029/2002GC000351.

Knutz, P. C., R. Zahn, and I. R. Hall (2007), Centennial-scale variability of the British Ice Sheet: Implications for climate forcing and Atlantic meridional overturning circulation during the last deglaciation, *Paleoceanography*, *22*, PA1207, doi:10.1029/2006PA001298.

Kohfeld, K. E., R. G. Fairbanks, S. L. Smith, and I. D. Walsh (1996), *Neogloboquadrina pachyderma* (sinistral coiling) as paleoceanographic tracers in polar oceans: Evidence from northeast water Polynya plankton tows, sediment traps, and surface sediments, *Paleoceanography*, *11*, 679–699, doi:10.1029/96PA02617.

Kucera, M., A. Rosell-Melé, R. Schneider, C. Waelbroeck, and M. Weinelt (2005), Multiproxy approach for the reconstruction of the glacial ocean surface (MARGO), *Quat. Sci. Rev.*, *24*, 813–819, doi:10.1016/j.quascirev.2004.07.017.

Kuijpers, A., M. S. Andersen, N. H. Kenyon, H. Kunzendorf, and T. C. E. van Weering (1998), Quaternary sedimentation and Norwegian sea overflow pathways around Bill Bailey Bank, northeastern Atlantic, *Mar. Geol.*, *152*, 101–127, doi:10.1016/S0025-3227(98)00066-8.

Lassen, S., E. Jansen, K. L. Knudsen, A. Kuijpers, M. Kristensen, and K. Christensen (1999), Northeast Atlantic sea surface circulation during the past 30–10 ^{14}C kyr B.P., *Paleoceanography*, *14*, 616–625, doi:10.1029/1999PA900029.

Lekens, W. A. H., H. P. Sejrup, H. Haflidason, J. Knies, and T. Richter (2006), Meltwater and ice rafting in the southern Norwegian Sea between 20 and 40 calendar kyr B.P.: Implications for Fennoscandian Heinrich events, *Paleoceanography*, *21*, PA3013, doi:10.1029/2005PA001228.

Lekens, W. A. H., H. Haflidason, H. P. Sejrup, A. Nygard, T. Richter, C. Vogt, and T. Frederichs (2009), Sedimentation history of the northern North Sea Margin during the last 150 ka, *Quat. Sci. Rev.*, *28*, 469–483, doi:10.1016/j.quascirev.2008.11.010.

Lowe, J. J., S. O. Rasmussen, S. Björck, W. Z. Hoek, J. P. Steffensen, M. J. C. Walker, Z. C. Yu, and INTIMATE Group (2007), Synchronisation of palaeoenvironmental events in the North Atlantic region during the Last Termination: A revised protocol recommended by the INTIMATE group, *Quat. Sci. Rev.*, *27*(1–2), 6–17, doi:10.1016/j.quascirev.2007.09.016.

Lund, S. P., M. Schwartz, L. Keigwin, and T. Johnson (2005), Deep-sea sediment records of the Laschamp geomagnetic field excursion (~41,000 calendar years before present), *J. Geophys. Res.*, *110*, B04101, doi:10.1029/2003JB002943.

Malmgren, B. A., M. Kucera, J. Nyberg, and C. Waelbroeck (2001), Comparison of statistical and artificial neural network techniques for estimating past sea surface temperatures from planktonic foraminifer census data, *Paleoceanography*, *16*, 520–530, doi:10.1029/2000PA000562.

McCartney, M. S. (1992), Recirculating components to the deep boundary current of the northern North Atlantic, *Prog. Oceanogr.*, *29*, 283–383, doi:10.1016/0079-6611(92)90006-L.

McDougall, I., and T. M. Harrison (1999), *Geochronology and Thermochronology by the $^{40}Ar/^{39}Ar$ Method*, 2nd ed., 288 pp., Oxford Univ. Press, Oxford, U. K.

Meese, D. A., A. J. Gow, R. B. Alley, G. A. Zielinski, P. M. Grootes, M. Ram, K. C. Taylor, P. A. Mayewski, and J. F. Bolzan (1997), The Greenland Ice Sheet Project 2 depth-age scale: Methods and results, *J. Geophys. Res.*, *102*, 26,411–26,423, doi:10.1029/97JC00269.

Meland, M. Y., T. M. Dokken, E. Jansen, and K. Hevrøy (2008), Water mass properties and exchange between the Nordic seas and the northern North Atlantic during the period 23–6 ka: Benthic oxygen isotopic evidence, *Paleoceanography*, *23*, PA1210, doi:10.1029/2007PA001416.

Morewood, N. C., P. M. Shannon, and G. D. Mackenzie (2004), Seismic stratigraphy of the southern Rockall Basin: A comparison between wide-angle seismic and normal incidence reflection data, *Mar. Pet. Geol.*, *21*, 1149–1163, doi:10.1016/j.marpetgeo.2004.07.006.

New, A. L., and D. Smythe-Wright (2001), Aspects of the circulation in the Rockall Trough, *Cont. Shelf Res.*, *21*, 777–810, doi:10.1016/S0278-4343(00)00113-8.

Nielsen, T., T. L. Rasmussen, S. Ceramicola, and A. Kuijpers (2007), Quaternary sedimentation, margin architecture and ocean circulation variability around the Faroe Islands, North Atlantic, *Quat. Sci. Rev.*, *26*, 1016–1036, doi:10.1016/j.quascirev.2006.12.005.

O'Reilly, B. M., P. M. Shannon, and P. W. Readman (2007), Shelf to slope sedimentation processes and the impact of Plio-Pleistocene glaciations in the northeast Atlantic, west of Ireland, *Mar. Geol.*, *238*, 21–44, doi:10.1016/j.margeo.2006.12.008.

Pardo-Igúzquiza, E., M. Chica-Olmo, and F. J. Rodríguez-Tovar (1994), CYSTRATI: A computer program for spectral analysis of stratigraphic successions, *Comput. Geosci.*, *20*, 511–584, doi:10.1016/0098-3004(94)90080-9.

Peck, V. L., I. R. Hall, R. Zahn, H. Elderfield, F. E. Grousset, and J. D. Scourse (2006), High resolution evidence for linkages between NW European ice sheet instability and Atlantic Meridional Overturning Circulation, *Earth Planet. Sci. Lett.*, *243*, 476–488, doi:10.1016/j.epsl.2005.12.023.

Peck, V. L., I. R. Hall, R. Zahn, F. E. Grousset, and J. D. Scourse (2007a), The relationship of Heinrich events and their European precursors over the past 60 ka BP: A multi-proxy ice-rafted debris provenance study in the North East Atlantic, *Quat. Sci. Rev.*, *26*, 862–875, doi:10.1016/j.quascirev.2006.12.002.

Peck, V. L., I. R. Hall, R. Zahn, and J. D. Scourse (2007b), Progressive reduction in NE Atlantic intermediate water ventilation prior to Heinrich events: Response to NW European ice sheet instabilities?, *Geochem. Geophys. Geosyst.*, *8*, Q01N10, doi:10.1029/2006GC001321.

Peck, V. L., I. R. Hall, R. Zahn, and H. Elderfield (2008), Millennial-scale surface and subsurface paleothermometry from the northeast Atlantic, 55–8 ka BP, *Paleoceanography*, *23*, PA3221, doi:10.1029/2008PA001631.

Perkins, H., T. S. Hopkins, S.-A. Malmberg, P.-M. Poulain, and A. Warn-Varnas (1998), Oceanographic conditions east of Iceland, *J. Geophys. Res.*, *103*, 21,531–21,542, doi:10.1029/98JC00890.

Peters, C., J. Walden, and W. E. N. Austin (2008), Magnetic signature of European margin sediments: Provenance of ice-rafted debris and the climatic response of the British ice sheet during Marine Isotope Stages 2 and 3, *J. Geophys. Res.*, *113*, F03007, doi:10.1029/2007JF000836.

Peters, C., W. E. N. Austin, J. Walden, and F. D. Hibbert (2010), Magnetic characterisation and correlation of a Younger Dryas tephra in North Atlantic marine sediments, *J. Quat. Sci.*, *25*, 339–347, doi:10.1002/jqs.1320.

Pflaumann, U., J. Duprat, C. Pujol, and L. Labeyrie (1996), SIMMAX: A modern analog technique to deduce Atlantic sea surface temperatures from planktonic foraminifera in deep-sea sediments, *Paleoceanography*, *11*, 15–35, doi:10.1029/95PA01743.

Prell, W. L. (1985), *The stability of low-latitude sea-surface temperatures: An evaluation of the CLIMAP reconstruction with emphasis on the positive SST anomalies*, 60 pp., Dep. of Energy, Washington, D. C.

Rashid, H., and E. A. Boyle (2007), Mixed-layer deepening during Heinrich events: A multi-planktonic foraminiferal delta O-18 approach, *Science*, *318*, 439–441, doi:10.1126/science.1146138.

Rasmussen, T. L., and E. Thomsen (2004), The role of the North Atlantic Drift in the millennial timescale glacial climate fluctuations, *Palaeogeogr. Palaeoclimatol. Palaeoecol.*, *210*, 101–116, doi:10.1016/j.palaeo.2004.04.005.

Rasmussen, T. L., E. Thomsen, L. Labeyrie, and W. T. C. E. van Weering (1996a), Circulation changes in the Faeroe-Shetland Channel correlating with cold events during the last glacial period (58–10 ka), *Geology*, *24*, 937–940, doi:10.1130/0091-7613(1996)024<0937:CCITFS>2.3.CO;2.

Rasmussen, T. L., E. Thomsen, W. T. C. E. van Weering, and L. Labeyrie (1996b), Rapid changes in surface and deep water conditions at the Faeroe margin during the last 58,000 years, *Paleoceanography*, *11*, 757–771, doi:10.1029/96PA02618.

Ruddiman, W. F. (1977), Late Quaternary deposition of ice-rafted sand in subpolar North Atlantic (lat 40° to 65°N), *Geol. Soc. Am. Bull.*, *88*, 1813–1827, doi:10.1130/0016-7606(1977)88<1813:LQDOIS>2.0.CO;2.

Ruddiman, W. F., and A. McIntyre (1981), Oceanic mechanisms for amplification of the 23,000-year ice-volume cycle, *Science*, *212*, 617–627, doi:10.1126/science.212.4495.617.

Salgueiro, E., A. H. L. Voelker, L. de Abreu, F. Abrantes, H. Meggers, and G. Wefer (2010), Temperature and productivity changes off the western Iberian margin during the last 150 ky, *Quat. Sci. Rev.*, *29*, 680–695, doi:10.1016/j.quascirev.2009.11.013.

Samson, S. D., and E. C. Alexander (1987), Calibration of the interlaboratory $^{40}Ar/^{39}Ar$ dating standard, MMhb1, *Chem. Geol. Isot. Geosci. Sect.*, *66*, 27–34, doi:10.1016/0168-9622(87)90025-X.

Sarnthein, M., P. M. Grootes, J. P. Kennett, and M. J. Nadeau (2007), ^{14}C reservoir ages show deglacial changes in ocean currents and carbon cycle, in *Ocean Circulation: Mechanisms and Impacts*, *Geophys. Monogr. Ser.*, vol 173, edited by A. Schmittner, J. C. H. Chiang, and S. R. Hemming, pp. 175–196, AGU, Washington, D. C.

Scourse, J. D., I. R. Hall, I. N. McCave, J. R. Young, and C. Sugdon (2000), The origin of Heinrich layers: Evidence from H2 for European precursor events, *Earth Planet. Sci. Lett.*, *182*, 187–195, doi:10.1016/S0012-821X(00)00241-7.

Scourse, J. D., A. I. Haapaniemi, E. Colmenero-Hidalgo, V. L. Peck, I. R. Hall, W. E. N. Austin, P. C. Knutz, and R. Zahn (2009), Growth, dynamics and deglaciation of the last British-Irish ice sheet: The deep-sea ice-rafted detritus record, *Quat. Sci. Rev.*, *28*, 3066–3084, doi:10.1016/j.quascirev.2009.08.009.

Sejrup, H. P., B. O. Hjelstuen, K. I. T. Dahlgren, H. Haflidason, A. Kuijpers, A. Nygård, D. Praeg, M. S. Stoker, and T. O. Vorren (2005), Pleistocene glacial history of the NW European continental margin, *Mar. Pet. Geol.*, *22*, 1111–1129, doi:10.1016/j.marpetgeo.2004.09.007.

Sierro, F. J., et al. (2009), Phase relationship between sea level and abrupt climate change, *Quat. Sci. Rev.*, *28*, 2867–2881, doi:10.1016/j.quascirev.2009.07.019.

Simstich, J., M. Sarnthein, and H. Erlenkeuser (2003), Paired $d^{18}O$ signals of *Neogloboquadrina pachyderma* (s) and *Turborotalita quinqueloba* show thermal stratification structure in Nordic Seas, *Mar. Micropaleontol.*, *48*, 107–125, doi:10.1016/S0377-8398(02)00165-2.

Smith, L. M., and J. T. Andrews (2000), Sediment characteristics in iceberg dominated fjords, Kangerlussuaq region, East Greenland, *Sediment. Geol.*, *130*, 11–25, doi:10.1016/S0037-0738(99)00088-3.

Stuiver, M., P. J. Reimer, E. Bard, J. W. Beck, G. S. Burr, K. A. Hughen, B. Kromer, F. G. McCormac, J. V. D. Plicht, and M. Spurk (1998), INTCAL98 radiocarbon age calibration, 24,000–0 cal BP, *Radiocarbon*, *40*, 1041–1083.

Svensson, A., et al. (2008), A 60 000 year Greenland stratigraphic ice core chronology, *Clim. Past*, *4*(1), 47–57, doi:10.5194/cp-4-47-2008.

van Aken, H. M. (2000), The hydrography of the mid-latitude northeast Atlantic Ocean II: The intermediate water masses, *Deep Sea Res., Part I*, *47*, 789–824, doi:10.1016/S0967-0637(99)00112-0.

van Kreveld, S. A., M. Sarnthein, H. Erlenkeuser, P. Grootes, S. Jung, M. J. Nadeau, U. Pflaumann, and A. Voelker (2000), Potential links between surging ice sheets, circulation changes and the Dansgaard-Oeschger cycles in the Irminger Sea, 60–18 kyr, *Paleoceanography*, *15*, 425–442, doi:10.1029/1999PA000464.

Vidal, L., L. Labeyrie, E. Cortijo, M. Arnold, J. C. Duplessy, E. Michel, S. Becquey, and T. C. E. Van Weering (1997), Evidence for changes in the North Atlantic Deep Water linked to meltwater surges during the Heinrich events, *Earth Planet. Sci. Lett.*, *146*, 13–27, doi:10.1016/S0012-821X(96)00192-6.

Voelker, A. H. L., M. Sarnthein, P. Grootes, H. Erlenkeuser, C. Laj, C. Mazaud, M.-J. Nadeau, and M. Schleicher (1998), Correlation of marine ^{14}C ages from the Nordic Seas with the GISP2 isotope record: Implications for radiocarbon calibration beyond 25 kyr, *Radiocarbon*, *40*, 517–534.

Voelker, A. H. L., L. de Abreu, J. Schönfeld, H. Erlenkeuser, and F. Abrantes (2009), Hydrographic conditions along the western Iberian margin during marine isotope stage 2, *Geochem. Geophys. Geosyst.*, *10*, Q12U08, doi:10.1029/2009GC002605.

Waelbroeck, C., J.-C. Duplessy, E. Michel, L. Labeyrie, D. Paillard, and J. Duprat (2001), The timing of the last deglaciation in North Atlantic climate records, *Nature*, *412*, 724–727, doi:10.1038/35089060.

Weinelt, M., E. Vogelsang, M. Kucera, U. Pflaumann, M. Sarnthein, A. Voelker, H. Erlenkeuser, and B. A. Malmgren (2003), Variability of North Atlantic heat transfer during MIS 2, *Paleoceanography*, *18*(3), 1071, doi:10.1029/2002PA000772.

Whittington, G., and A. M. Hall (2002), The Tolsta Interstadial, Scotland: Correlation with D-O cycles GI-8 to GI-5?, *Quat. Sci. Rev.*, *21*, 901–915, doi:10.1016/S0277-3791(01)00068-3.

Wilson, L. J., and W. E. N. Austin (2002), Millennial and sub-millennial-scale variability in sediment colour from the Barra Fan, NW Scotland: Implications for British ice sheet dynamics, in *Glacier-Influenced Sedimentation on High-Latitude Continental Margins*, edited by J. A. Dowdeswell and C. Ó. Cofaigh, *Geol. Soc. Spec. Publ.*, *203*, 349–365, doi:10.1144/GSL.SP.2002.203.01.18.

E. Colmenero-Hidalgo, Facultad de Ciencias Biológicas y Ambientales, Universidad de León, Campus de Vegazana S/N E-24071, León, Spain.

I. R. Hall, School of Earth and Ocean Sciences, Cardiff University, Main Bldg., Park Place, Cardiff CF10 3AT, UK. (hall@cardiff.ac.uk)

S. R. Hemming, Lamont-Doherty Earth Observatory, Columbia University, Palisades, NY 10964, USA.

V. L. Peck, British Antarctic Survey, High Cross, Madingley Road, Cambridge CB3 0ET, UK.

R. Zahn, Institut de Ciencia i Tecnología Ambientals, Departament de Física, Universitat Autónoma de Barcelona, Edifici Cn, Campus UAB, E-08193 Bellaterra, Spain.